Energy & Environmental Science

Accepted Manuscript

ROYAL SOCIETY OF CHEMISTRY

www.rsc.org/ees

Energy Environmental Science

RSCPublishing

Review

Olivine $LiFePO_4$: the remaining challenges for future energy storage

Cite this: DOI: 10.1039/xoxxoooooox

Jiajun Wang, [a]† and Xueliang Sun [a]*

Received ooth January 2012,
Accepted ooth January 2012

DOI: 10.1039/xoxxoooooox

www.rsc.org

Since the first report in 1997, olivine $LiFePO_4$ has been considered as the most competitive cathode material for electric vehicles due to its high thermal stability and safety, therefore, numerous efforts have been made to understand and improve the performance of $LiFePO_4$. In spite of some breakthrough advances, large-scale application of $LiFePO_4$ batteries in transportation still meets many technical obstacles. In our previous review paper, we mainly discussed carbon coating technology, one most important breakthrough in $LiFePO_4$ development. In combination with the latest advances in the $LiFePO_4$ field, here we provide an updated overview of current research activities and highlight some key challenges (fast-charging, lithiation-delithiation mechanism, surface chemistry stability, etc.) for future $LiFePO_4$ development. These obstacles necessitate the understanding of $LiFePO_4$ under *in situ* or *in operando* condition; as a result, the application of advanced synchrotron X-ray technology (mainly imaging tools) is also briefly summarized. In addition, considering to the new research trend in next-generation battery system, the up-to-date understanding and exploration of olivine phosphate for Na-ion batteries also expect new research hotspots in energy storage field. A couple of practical issues with strong industrial interests are also included. .

Broader context

Rechargeable batteries can effectively store electrical energy as chemical energy, and release it as needed, providing a good choice for electric vehicle (EV) applications. Naturally, safety concerns are the key issue for the application of battery technology in EVs. Olivine $LiFePO_4$ is considered to be the most promising cathode material for lithium-ion batteries due to its environmental friendliness, high cycling performance and safety characteristics. Some important breakthroughs in recent years have allowed its successful commercialization. In spite of its success, the commercial application of $LiFePO_4$ batteries in EVs has still been hindered by some technological obstacles. Here we provide an update on our previous review, and overview the most significant advances dealing with the remaining challenges for this promising battery material. New research direction and future trends are also discussed.

1. Introduction

Since the first report in 1997 by Goodenough et al,[1] lithium iron phosphate has become one of the hottest cathode materials in battery research field. In particular, in recent years the considerable demands for high safety and high-performance large scale energy storage system in electric vehicles has inspired numerous research efforts to optimize this cathode material, which has been summarized in several excellent review papers. [2-5] With the size-reduction to the nanoscale and carbon coating strategies,[6-8] the poor intrinsic electronic and ionic conductivity has been enormously improved and commercial $LiFePO_4$ batteries have begun to be used in electric vehicles. Despite the superior thermal safety, high reversibility and acceptable operating voltage (3.45 vs. Li^+/Li) make it more competitive than other cathode materials; there is still a long way before using $LiFePO_4$ for large-scale application in electric vehicles. Many technical challenges remain unsolved.

One challenge is related to the demands of fast-charging for EV's batteries.[9] Compared to the electronic conductivity, the ionic conductivity or lithium-ion diffusion plays a dominate role in determining the electrochemical reaction kinetics. It is widely accepted that the electrochemical delithiation reaction proceeds via a two-phase process between the two end members of $LiFePO_4$ and $FePO_4$, [10] and lithium ions diffuse along 1-dimensional pathway with a preferential (010) direction,[11] hindering the fast lithium ion insertion/extraction. Although the rate performance of $LiFePO_4$ has been improved by shortening the diffusion distance with size reduction, [12,13] it is still not able to satisfy the high rate expectations of EVs. Despite the success of some conventional engineering methods, a breakthrough in high rate performance is needed, which heavily relies on the fundamental understanding of the lithium diffusion kinetics and the underlying phase transformation mechanism. The exploration and development of a number of *in situ* experimental techniques,[14-18] particularly in recent years, poses new opportunities to shed light on previous controversial

models and suggest possible solutions to high rate performance. An obvious trend is that of a single-phase mechanism or solid solution models have been confirmed by various different experimental evidence,[19-22] which enrich previous mechanism elucidation and also provide new theoretical guidelines for further high rate $LiFePO_4$ battery materials.

The other challenge is surface chemistry stability in $LiFePO_4$. In general, due to the strong P-O covalent bonds in the olivine structure which prohibit oxygen release, $LiFePO_4$ is considered to have a superior thermal stability. Nevertheless, the actual $LiFePO_4$ batteries are not always as stable as expected. Performance degradation always occurs with electrochemical cycling,[23,24] which is considered to be due to moisture contamination. Many research interests have been put on understanding the surface chemistry change or aging process when moisture contamination is present including storage and electrochemical working conditions.[24-26] In addition, considering the strong reducing environment and high temperatures found in the carbon coating process, possible surface chemistry change of $LiFePO_4$ has attracted much attention because $LiFePO_4$ surface and the interface between carbon and $LiFePO_4$ directly affect electronic and ion conductivity.

Another research trend is development of novel olivine family for next-generation battery systems. Because of their low cost and wide availability, sodium ion batteries have recently been pursued as the potential alternative of current lithium-ion batteries.[27,28] Encouraged by the tremendous success of olivine $LiFePO_4$ in lithium-ion batteries, the analogous $NaFePO_4$ has been expected to show similar properties as $LiFePO_4$, however, this is not always the case. Recent studies show a significant difference between $NaFePO_4$ and $LiFePO_4$, including electrochemical properties (capacity, reversibility, cycle performance), the phase transformation mechanism, and synthesis routes.[29,30]

In our previous review,[31] we focused on the progress and development of carbon coating methods for $LiFePO_4$. Considering this popular battery material and its recent important progress, here we present an updated review mainly based on the latest two year's literature and extend our discussion to focus on new aspects of the aforementioned actively studied topics in olivine $LiFePO_4$, including performance optimizing strategies, understanding of the insertion/extraction mechanism via *in situ* methods, surface chemistry stability and future olivine phosphate for sodium ion batteries. Some perspectives and suggestions with regard to future research directions and challenges are also provided.

2. Strategies for performance improvement

2.1 Optimizing carbon coating

Carbon coating on $LiFePO_4$ is a widely accepted method to improve a battery material's conductivity. Generally, carbon coating process involves mixing battery materials with various carbon precursors and a proceeding high-temperature thermal treatment. This approach is simple, feasible, and suitable for large-scale industrial production. However, the control of a uniform coating layer and improving the carbon quality is still very challenging. Too thin of a carbon coating layer cannot cover the active material uniformly, but too thick of a carbon coating also limits lithium ion diffusion and decreases the volumetric energy density of battery materials. To meet the demands for high performance battery materials, current carbon coating technology still needs to be further improved.

First, to optimize carbon coating quality for $LiFePO_4$, the selection of a high quality carbon source is critical.[32,33] A variety of carbon sources with different chemical and physical properties have been applied to carbon coating process for $LiFePO_4$. Some classic carbon sources include some organic, such as glucose, citric acid and lactose, and some inorganic, such as acetylene black, carbon nanotubes, and graphene. Organic carbon sources are advantageous to form homogeneous carbon coating layer and a well control carbon layer structure (thickness, homogeneity, full coverage) during the pyrolysis process at high temperatures, but carbon quality (conductivity, graphitized degree) is hard to control. Inorganic carbon provide the opposite advantages and disadvantages. With selection of high quality inorganic carbon such as carbon nanotubes and graphene, the entire $LiFePO_4$ electrode can be composed of a 3D conductive network, but local conductive paths in individual $LiFePO_4$ particles (particle surface) may still need to be provided with small amounts of an organic carbon coating. The combination of the advantages of both organic and inorganic carbon sources is more promising for high performance C/$LiFePO_4$ composites.[34]

Second, to maximize the electronic conductivity improvement, a uniform carbon nanolayer with full coverage on $LiFePO_4$ should be firstly achieved, which is a challenge for many carbon coating methods. Despite this, some *in situ* carbon coating methods such as self-polymerization of dopamine or resorcinol–formaldehyde gel can result in a uniform carbon coating layer on $LiFePO_4$, however, a more economic and feasible method is still high desirable.[35,36] Recently, a novel carbon coating method via physical evaporation and deposition of carbon under vacuum was reported.[37] By continuous agitation of the sample coupled to rotation and tilting of sample holder, a homogeneous and uniform carbon coating layer can be obtained. The carbon coating thickness can be controlled with the deposition time and the physical properties (the conductivity and graphitization degree) of carbon coating are proved to be similar to those of traditional high-temperature treatment method. Despite this, further improvement is still needed for further large-scale production, however, this method provides a new route to achieve a high-quality carbon coating on $LiFePO_4$ battery materials.

Third, further modification of the carbon coating layer via nitrogen doping or co-coating (hybrid coating) provides feasible strategies to optimize the carbon coating for $LiFePO_4$. A nitrogen-doped carbon layer has proven to improve electrical contact/conductivity and prevent $LiFePO_4$ aggregation, thus treated $LiFePO_4$ was shown to exhibit a superior rate capability and capacity retention.[38] Because of the hydrophilic properties of nitrogen doping, our previous work also indicates that nitrogen doped carbon nanotubes allow more uniform dispersion of carbon nanomaterials and thus enhance electronic contact of $LiFePO_4$.[39] Furthermore, nitrogen atoms also may contribute additional electrons, providing electron carriers for the conduction band and further improving electronic conductivity of $LiFePO_4$. In addition to electronic conductivity improvement, nitrogen also may induce defects to lower the activation energy of lithium ion diffusion, enhancing lithium ion diffusion kinetics. Therefore, an improved rate performance can be expected by nitrogen doped carbon coating. The other modification strategy for carbon coating is co-coating carbon with metal oxides or ionic conductors. Metal oxide co-coating may improve charge transfer resistance, and more importantly,

it can improve surface chemical stability of $LiFePO_4$ by consuming HF created by moisture contamination.[40-42] Ionic conductor (Li_3PO_4 and $CePO_4$ et al.) co-coating allows faster lithium ion diffusion. Combining with highly electronic conductivity carbon coating, this hybrid coating improves rate performance and low temperature performance of $LiFePO_4$.[43,44] However, the optimized ratio of the ionic/electronic conductor and a controlled hybrid coating method are still challenges for practical $LiFePO_4$ production.

Fourth, in addition to optimizing the carbon coating layer, another strategy to improve $LiFePO_4$ performance is the fabrication of additional carbon structures to make up for the deficiencies of the inhomogeneous carbon coating layer. By creating interconnected open pores for electrolyte penetration and limiting $LiFePO_4$ agglomeration, 3D carbon structures enable faster inter-particle lithium-ion and electron transfer, leading to high utilization of $LiFePO_4$ particles and good columbic efficiency.[45,46] For example, Ni et al recently introduced carbon coated $LiFePO_4$ to a porous carbon structure and fabricated a 3D carbon coated $LiFePO_4$-porous carbon composites. $FePO_4{\cdot}2H_2O$ precursor was first deposited into the porous carbon matrix, and followed by an *in situ* transformation into carbon coated $LiFePO_4$ with $CH_3COOLi{\cdot}2H_2O$ and sucrose as the lithium and carbon sources, respectively. As a result, carbon coated $LiFePO_4$ particles were well dispersed into the porous carbon matrix. The double carbon structure (carbon nanolayer on the $LiFePO_4$ particles and additional carbon matrix) created a 3D conductive network, provides fast ionic and electronic conduction, contributing to a high rate performance of $LiFePO_4$.[47]

Finally, a porous carbon coating layer is highly expected to improve the performance of $LiFePO_4$. In recent years, the advances in $LiFePO_4$ electric vehicle batteries have placed a higher demand on carbon coatings. In general, the main functions of the carbon coating for $LiFePO_4$ are the improvement of the electronic conductivity and the control of the particle size growth at high temperatures. However, to practically use $LiFePO_4$ for EVs, carbon coating is also expected to enhance ionic conductivity in order to achieve a high rate performance. Therefore, a recent research trend in carbon coating has been to develop a porous carbon structure on $LiFePO_4$ which enables the storage of sufficient electrolyte to maximize the electrode reaction interface, and most importantly, provide a fast lithium ion transfer pathway.[48,49] Textural structured carbon aerogels with a large amount of micropores (nanometers) and mesopores (ten of nanometers) are ideal carbon sources, and have attracted much attention recently.[50] With optimizing of the experimental parameter, tuning pore size and controlling pore distribution, these porous carbon sources can be expected to play an increasing role in the structural design of future high rate $LiFePO_4$ materials.

2.2. Advanced carbon composite

In addition to the conventional carbon coating via pyrolysis of organic carbon sources, in recent years, the introduction and synthesis of advanced carbon materials such as graphene and carbon nanotubes has been widely applied to the improvement of $LiFePO_4$ conductivity due to its unique character and superior electronic conductivity.

Graphene. Graphene, a monolayer of SP^2-bonded carbon atoms or one monolayer of graphite has attracted considerable attention as an advanced carbon additive. The structural flexibility, large specific surface area, high mechanical strength, and superior electric conductivity of graphene can build a highly effective 3D conductive network for $LiFePO_4$, increase inter-particle electric contact, and therefore improve electrochemical performance of $LiFePO_4$. [51,52] Based on these unique advantages, numerous studies on graphene modified $LiFePO_4$ have been reported in recent years,[53-56] and the graphene/$LiFePO_4$ composites indeed show improved electrochemical performance. Currently, it is generally accepted that the enhanced electrochemical performance of graphene/$LiFePO_4$ is attributed to the inherent features of graphene (excellent electronic conductivity, high surface area, etc). In addition, the introduction of 2D graphene can lead to more uniform $LiFePO_4$ particle dispersion than conventional carbon additives such as acetylene black, resulting in high electrochemical performance.[57] Furthermore, graphene may lead to additional capacity for the cathode. A recent report shows that graphene-modified $LiFePO_4$ can charge beyond its theoretical capacity. Hu et al applied 2wt% graphene to wrap the commercial carbon coated $LiFePO_4$ resulting in a capacity of 208 mAh/g (the theoretical value is 170 mAh/g for $LiFePO_4$), as shown in Fig. 1. The authors attributed the extra capacity to the reversible redox reaction between lithium ions in the electrolyte and exfoliated graphene flakes. If this is the case, this unique feature is also likely applicable to other battery materials. [58]

In spite of these unique features of graphene, the practical application of graphene faces too many challenges. The first challenge is the easy aggregation and poor dispersion of 2D graphene sheets in common solvents due to its hydrophobic nature, which significantly decreases its advantages.[59,60] Our group studied the impact of stacked and unfolded graphene on $LiFePO_4$ performance. It was found that, compared with stacked graphene with a wrinkled structure (synthesized by thermal reduction of graphene oxide), unfolded graphene (synthesized by hydrazine

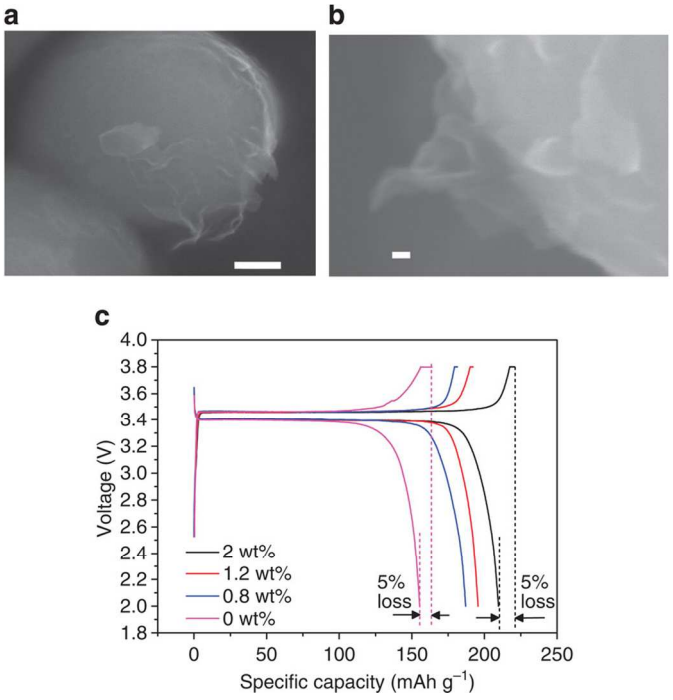

Fig. 1 Morphology and electrochemical performance of graphene/$LiFePO_4$ composite. (a,b) SEM images of graphene/$LiFePO_4$. Scale bar, 100 nm and 10 nm in a and b, respectively. (c) The first charge/discharge profile at 0.1 C for graphene/$LiFePO_4$ composite with various graphene-loadings (0, 0.8, 1.2 and 2 wt%). Reproduced with permission from ref. 58. Copyright 2014, Nature Publishing Group.

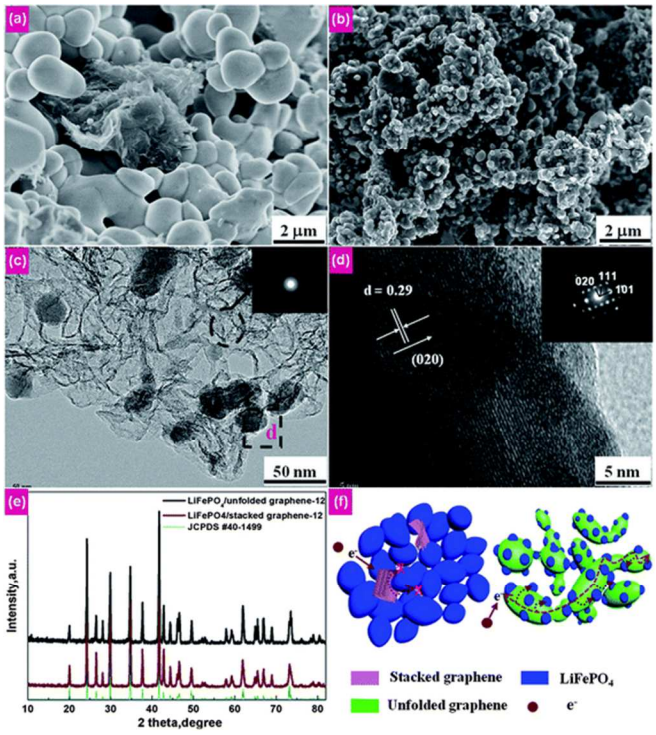

Fig. 2 SEM images of (a) stacked graphene/$LiFePO_4$ composites and (b) unfolded graphene/$LiFePO_4$ composites. (c) TEM image of LiFePO4–unfolded graphene composites. (d) High-resolution TEM image and SAED pattern (inset) of an individual $LiFePO_4$ nanoparticle on unfolded graphene (square area in (c)). (e) XRD spectrum of the unfolded graphene /$LiFePO_4$ and stacked graphene/$LiFePO_4$ composites. (f) Electron-transfer pathway for the stacked graphene/$LiFePO_4$ and unfolded graphene /$LiFePO_4$ composites. Reproduced with permission from ref. 61. Copyright 2014, The Royal Society of Chemistry.

reduction of graphene oxide in solution) enables $LiFePO_4$ to well disperse so that individual $LiFePO_4$ particles are attached to the conductive layer, leading to higher electronic conductivity and performance as shown in Fig. 2.[61] To improve graphene dispersion in solutions, similar to carbon nanotubes, functioning treatment with a strong oxidizing agents is a common strategy to create hydrophilic carboxyl groups and surface defects.[62-64] However, this violent method also destroys the intact structure of graphene, leading to some loss of its unique mechanical, chemical and physical properties. A mild surface treatment method is highly expected to make full use of its advantages for battery materials.[65,66] Rhodanineacetic acid-pyrene (RAAP) was recently used to functionalize graphene nanosheets due to the strong π-π stacking force between RAAP and thermally exfoliated graphene. As a result, RAAP molecules were well dispersed on graphene nanosheet and the resulted graphene is negative charged. With the charge attraction, Fe^{2+} ions and PO_4^{3-} were adsorbed onto RAAP-modified graphene subsequently to form $FePO_4$/graphene hybrids. After mixing with $LiCH_3COOH$, the finial $LiFePO_4$/graphene composite was obtained by a thermal reduction process. With this strategy, $LiFePO_4$ particles can be directly grown on graphene with good electronic contact, leading to high rate capability and capacity retention upon cycling.[67] In addition, nitrogen doping is also a facile method to improve graphene dispersion in solutions.

Another challenge for graphene is the development of a simple and facile synthesis method. Most of graphene-related $LiFePO_4$ synthesis method involves complex and time-consuming synthesis processes, such as high temperature post-heating and extensive reflux reactions.[68-70] Although some approaches for mass production of graphene have recently been reported, [71,72] a rapid, economic and feasible approach with high yield of well crystalline graphene/$LiFePO_4$ material is highly desirable. Microwave assisted synthesis enables graphene nanosheet encapsulated $LiFePO_4$ within a few minutes at low temperatures without any post annealing treatments. This approach makes it possible for the large-scale industrial production of graphene/$LiFePO_4$ composites in the near future.[73] In addition, an ultrasonic-assisted rheological phase method in combination with a carbothermal reduction reaction was also recently developed to synthesize a graphene/$LiFePO_4$ composite. The rheological approach can decrease the calcination temperature and save treatment time. Meanwhile, the sucrose pyrolysis produces an additional carbon coating on the $LiFePO_4$, improving the carbon conductive network for $LiFePO_4$.[74] More recently, an *in situ* pyrolysis and catalytic graphitization approach to synthesize graphene-decorated $LiFePO_4$ was developed.[75] Glucose and a trace amount of $FeSO_4$ were used as the graphene source and catalyst precursors, respectively. With a solid state reaction, graphene formed a uniform coating layer on the $LiFePO_4$ nanoparticles. Because of the graphene conductive network, the obtained graphene-$LiFePO_4$ showed a superior specific capacity of 167.7 mAh/g and high rate performance with 94.3 mAh/g at 100 C.

Besides the dispersion and feasible synthetic methods, in practical application of graphene in $LiFePO_4$, some other issues should be also considered. One is how to increase the interaction and bonding between $LiFePO_4$ and graphene. Encapsulating $LiFePO_4$ on graphene nanosheets with chemical bonding was recently achieved by a self-assembly method. Luo et. al., modified $LiFePO_4$ particles by surface grafting amino- propyltrimethoxysilane to cover the surface with amino-groups. [76] With the formation of peptide bonds between amino-groups on $LiFePO_4$ and the carboxyl-groups on graphene, $LiFePO_4$ particles were successfully self-assembled on the graphene surface and formed a graphene oxide encapsulated $LiFePO_4$ composite. With the following reduction treatment, a graphene/$LiFePO_4$ composite with strong bonding and superior conductive network was formed, contributing to a high rate capability (70% capacity retention at 50C) and excellent cycle performance (8.6% capacity loss after 950 cycles at 10C). Another concern in the practical application of graphene with $LiFePO_4$ is lithium ion diffusion through graphene. Despite $LiFePO_4$ conductivity being significantly improved with the addition graphene, lithium ions may not easily pass through the carbon atom array of the 2D graphene sheets as expected. To favor lithium ion diffusion, modifying graphene sheets to produce more porosity allows rapid lithium ion diffusion, contributing to high rate performance of $LiFePO_4$. For example, Ha et. al. applied KOH activation to synthesize chemically activated graphene which provided a porous continuous conductive network, contributing to the superior electron transfer and fast lithium ion diffusion for $LiFePO_4$.[77]

Carbon nanotubes. In addition to graphene, carbon nnaotubes are another widely studied carbon material. Because of their inherent network structure, carbon nanotubes are generally used for $LiFePO_4$ to form three dimensional conductive networks, bridging the active particles. Incorporation of CNTs into $LiFePO_4$ has demonstrated enhanced capacity and rate performance for $LiFePO_4$.[78-80] When $LiFePO_4$ is combined with a CNT network, the conductive network facilitates charge mobility between the $LiFePO_4$ particles, contributing to the improved electrochemical performance of the entire $LiFePO_4$ electrode. By comparison, without an effective conductive network, charge distribution in the conventional

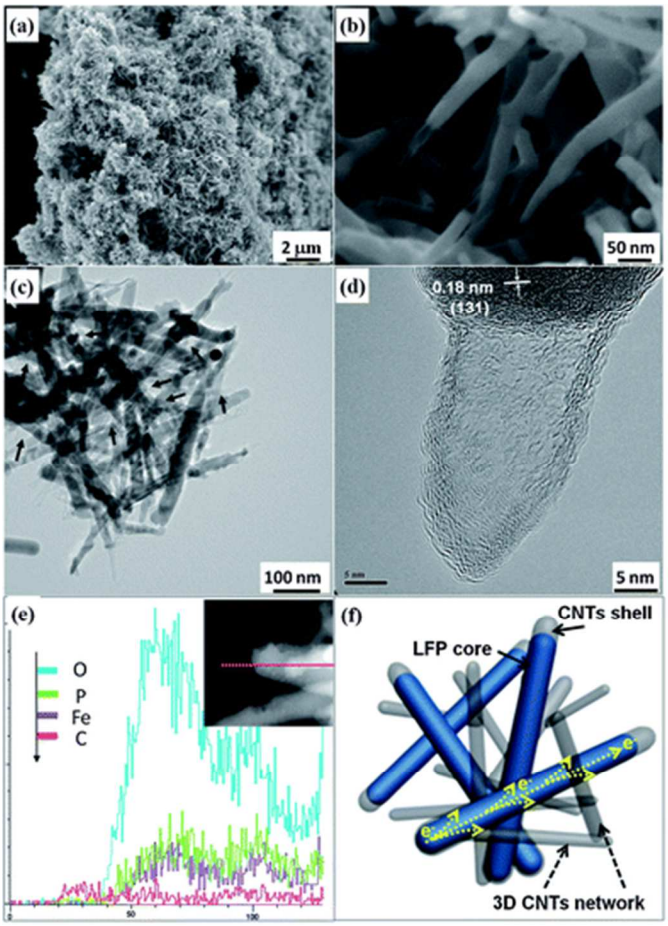

Fig. 3 (a and b) SEM images of the needle-like CNTs/$LiFePO_4$. (c) TEM image of the core–shell nanowires, and (d) the corresponding HRTEM image of a CNTs/$LiFePO_4$ nanowire. (e) EDX line profile of a CNTs/$LiFePO_4$ core–shell nanowire. (f) Schematic illustration of CNTs/ $LiFePO_4$ core–shell nanowires. Reproduced with permission from ref. 86. Copyright 2014, The Royal Society of Chemistry.

C/$LiFePO_4$ electrode may be localized or trapped at grain boundaries inside the electrode, leading to local low performance.[81]

In most CNTs-$LiFePO_4$ composites, CNTs are randomly incorporated with $LiFePO_4$, which may not make full use of CNTs conductive network because of the poor dispersion of CNTs in solutions owing to its high van der Waals forces.[82] Therefore, some functionalization methods have been developed on carbon nanotubes to improve the dispersion in $LiFePO_4$.[83,84] For example, poly(ethylene glycol) (PEG) was used to functionalize CNTs for $LiFePO_4$. In addition to the improved dispersion of CNTs in $LiFePO_4$ particles, lithium ion diffusion in PEG-modified CNTs-$LiFePO_4$ electrode increased 2 orders of magnitude, compared to the conventional $LiFePO_4$-acetlyene black electrode. [88]

Another solution to avoid carbon nanotube aggregation is via the *in-situ* growth CNTs with $LiFePO_4$. Our group developed an *in- situ* self-catalyzed formation of core-shell CNTs-$LiFePO_4$ nanowires (Fig. 3).[86] This novel composite was fabricated with two steps, a sol-gel route to form the one-dimensional $LiFePO_4$ precursor and a solid state step to form core-shell CNT-$LiFePO_4$ nanowires. The CNT network was formed via the self-catalyzed reaction where Fe^{2+} in the composite catalyzes the CNTs growth. The direct growth of CNTs from the composite effectively enhances the electronic conductivity. Meanwhile, the formation of CNTs also restricts the *in situ* crystallite growth of $LiFePO_4$ nanowires, controlling the nanowire size, which is important for the high rate performance of $LiFePO_4$. These 3D CNT-$LiFePO_4$ nanowires delivered a capacity of 160 mAh/g at 17 mA/g and 65 mAh/g at 8500 mA/g.

In addition to graphene and carbon nanotubes, some other carbon structure has also been employed in $LiFePO_4$ composites. Mesoporous carbon materials with hierarchical structure have high porosity, thus may facilitate lithium ion diffusion, shorten the diffusion paths, and increase the interfacial contact between electrolytes and $LiFePO_4$. For example, Wang et. al. developed a nanocasting technique to synthesize a mesoporous $LiFePO_4$/C nanocomposite.[87] The mesoporous structure improved electronic/ionic contact, improved the mass and charge transfer capabilities, and delivered a high rate performance. Wu et al developed another facile approach to obtain mesoporous a carbon nanosheet-$LiFePO_4$ composite via an *in situ* soft-template method.[88,89] The mesoporous carbon with high porosity served as both an electron and lithium ion conductive network, contributing to an excellent rate capability. In spite of these superior performance, a feasible and low-cost synthesis route to the large-scale production of these advanced carbon materials, especially the porous carbon structure, is still very challenging for current battery material applications.

2.3. Morphology control

Decreasing the size of $LiFePO_4$ particles to the nanoscale enables higher power density, which is mainly attributed to the shortened ion diffusion pathways inside the 1D channels of $LiFePO_4$.[90,91] However, the size reduction also adversely affects the tap density and volumetric energy density, and the high surface area increases the undesirable electrode/electrolyte reactions, which leads to a poor cycling performance. Furthermore, the unexpected anti-site defects often accompany the size-reduction during $LiFePO_4$ synthesis.

Currently, morphology tailoring and controlled synthesis have attracted increased attention to improve the rate performance of $LiFePO_4$. In general, hydrothermal methods at low temperatures allow well controlled $LiFePO_4$ size and morphology, but the obtained material generally shows poor electrochemical performance because of the presence of antisite defects in the crystal structure.[92] The iron occupancy on the M1 site is considered to be an antisite defect, which block lithium ion diffusion pathway through the 1D channel along the (010) direction in $LiFePO_4$ crystal structure, a process known as channel blocking. The formation of these defects is due to the faster introduction rates of iron than lithium into the crystalline structure during the synthesis process. To guarantee an ideal crystalline structure for a high capacity, only when all the lithium is introduced into the crystalline structure, the defects will be suppressed. To achieve this, some common strategies include extending the synthesis time, higher synthesis temperatures and a post-treatment at high temperatures.[93] However, these methods also result in unexpected particle growth. Recently, it was found that the solvent plays an important role in controlling antistite defects. Some solvents with low dielectric constants (such as ethylene glycol and ethanol) can reduce the concentration of Fe-Li anti-site defects. For example, using ethanol as the sole solvent via a solvothermal process, $LiFePO_4$/C was highly crystalline and exhibited less than 1% anti-site defects, which provides an alternative feasible route to limit the defects.[94]

In addition to suppressing anti-site defects, the orientation of $LiFePO_4$ particles tailored by morphology control also plays an

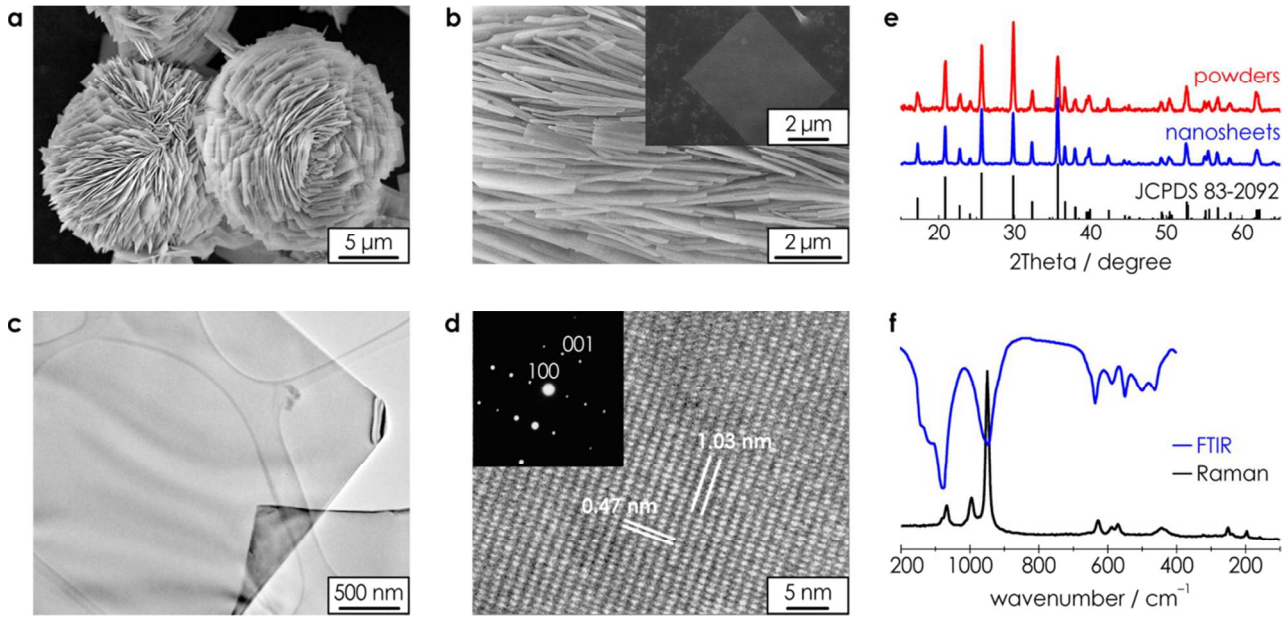

Fig. 4 Characterization of $LiFePO_4$ nanosheets. (a) Representative SEM image of the $LiFePO_4$ particles; (b) SEM image of the accumulated nanosheets. (c) TEM and (d) HRTEM image and ED pattern of the $LiFePO_4$ nanosheets. (e) XRD patterns of $LiFePO_4$ particles and exfoliated $LiFePO_4$ nanosheets. (f) Raman (black) and FTIR (blue) spectra of the as-exfoliated $LiFePO_4$ nanosheets. Reproduced with permission from ref. 101. Copyright 2014, American Chemical Society.

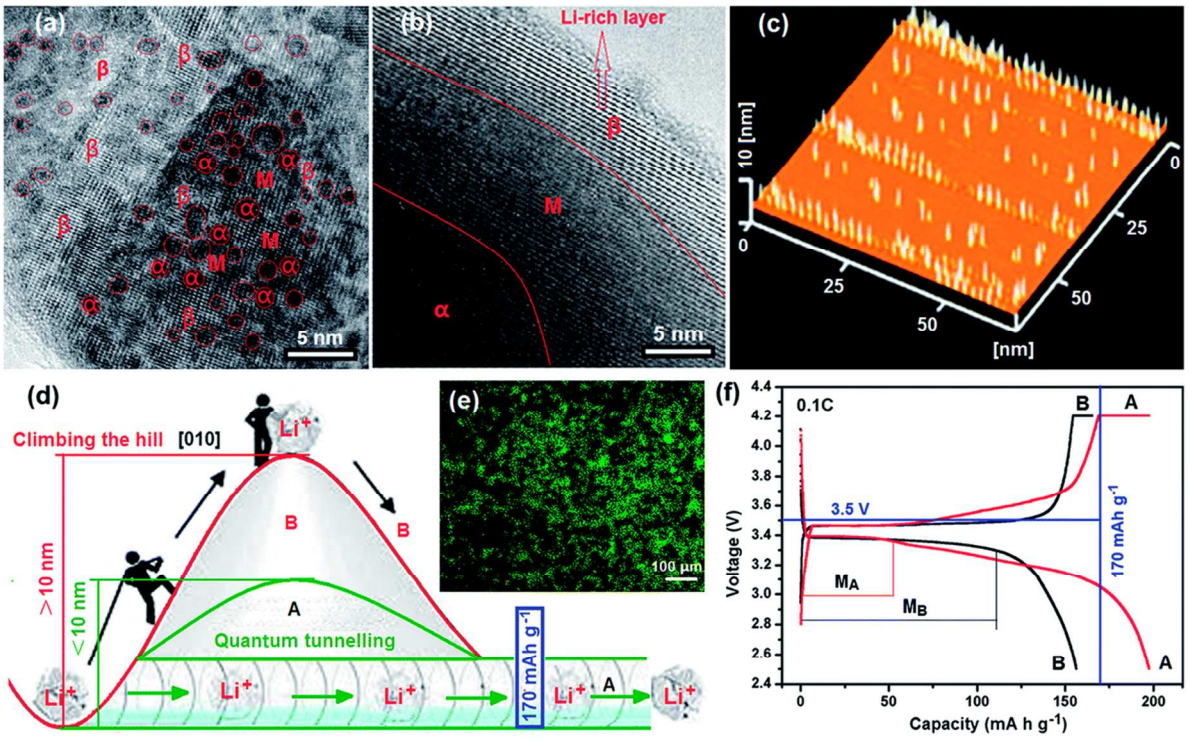

Fig. 5 Characterizations of high-energy $LiFePO_4$ quantum dots (HEQDs). (a) HRTEM image of HEQDs embedded in a $LiFePO_4$ nanosheet. (b) HRTEM image of a commercial $LiFePO_4$ particle. (c) AFM image of the size and height distributions of HEQDs embedded in a $LiFePO_4$ nanosheet. (d) Li ion pathways in the commercial sample (B) and mesoporous biocarbon nanowire coated $LiFePO_4$ (MBCNW-LFP-HEQDs) (A). (e) Fluorescent image of the MBCNW-LFP-HEQD-2 sample, (f) The first discharge/charge curves of the MBCNW-LFP-HEQD-2 cathode (A) and the commercial cathode (B) at 0.1 C rate. Reproduced with permission from ref. 104. Copyright 2014, The Royal Society of Chemistry.

important factor in improving the kinetics of the lithium ion extraction/insertion process. The 1D lithium diffusion pathways along the (010) direction suggest that the synthesis of thin and well dispersed $LiFePO_4$ nanostructures with a large (010) surface area would enhance its rate performance. Indeed, calculations based on the electronic structure of $LiFePO_4$

indicate that the low energy surfaces can dominate in the equilibrium shape.[95] Therefore, numerous efforts have been made to synthesize large surface area $LiFePO_4$ materials along their b axes to favor lithium ion diffusion.[96,97] It is well known that, at thermodynamic equilibrium state, each facet's surface area in a crystal depends on its free surface energy.[98] However, the preference of crystal facets in $LiFePO_4$ is also linked with the properties of the solvent. Currently, most control of the $LiFePO_4$ (010) crystal facets are achieved with the solvothermal conditions, typically with ethylene glycol as the solvent.[99,100] The binding energy of a solvent, which is defined as the energy difference after the absorption of solvent molecules, is considered to play a decisive role in facet control of $LiFePO_4$. A more recent report indicated that, when compared with ethylene glycol, the use of diethylene glycol is more favorable for (010) facet formation due to the more stable binding geometry. The directional alignment of diethylene glycol molecules may take place at the (010) facet and produce a long chain due to hydrogen bonds between diethylene glycol molecules, thereby making the formed (010) surfaces more stable. As a result, single-crystalline, (010)-oriented $LiFePO_4$ nanosheets (30−60 nm thick) were successfully synthesized by the solvothermal method with a diethylene glycol solvent, as shown in Fig. 4.[101] With an ionic liquid solvothermal method, a controllable growth of the (010) facet of $LiFePO_4$ with high rate capability can be also obtained.[102]

Most conventional morphological control is based on a variety of nanostructures such as nanowires, nanoparticles, nanosheets and core-shell structure. In particular, the core-shell structured $LiFePO_4$/carbon composite allow fast lithium ion and electron transportation, enabling high electrochemical performance. For example, with in situ polymerization method, Zhou et al designed $LiFePO_4$/carbon nanocomposite with core-shell structure and the obtained $LiFePO_4$ shows high rate capability and long life cycle.[103] In recent years, some new concepts have been introduced showing potential for future $LiFePO_4$ development. Quantum dots (QDs), a tiny particle containing only a small number of atoms, have extremely high surface-to-mass ratio. Because surface atoms generally possess higher energy of delocalized electrons and are kinetically more active than interior atoms, QDs can generally exhibit superior properties. Recently, Zhang et al synthesized high-energy quantum dots (HEQDs) in ultra-thin $LiFePO_4$ nanosheets.[104] It was found that the electrons and lithium ions can be easily transported to the HEQDs due to its tunneling barrier, as shown in Fig. 5. This novel $LiFePO_4$ nanostructure provides more storage sites of lithium ions and shows the superior discharge capacity and an ultra-high coulombic efficiency. In recent years, atomic layer deposition (ALD) has attracted much attention as a novel technique to engineer nanostructures for energy materials. Owing to the unique capability to tune nanostructures at the atomic scale, our group recently successfully developed this technique to deposit $LiFePO_4$ on carbon nanotubes (CNT). The obtained $LiFePO_4$/CNT exhibits exception battery performance, including superior rate capability, power density and long lifetime. The success of this technique in $LiFePO_4$ also has tremendous impact on future 3D all-solid state batteries and next-generation advanced battery systems (Fig. 6).[105]

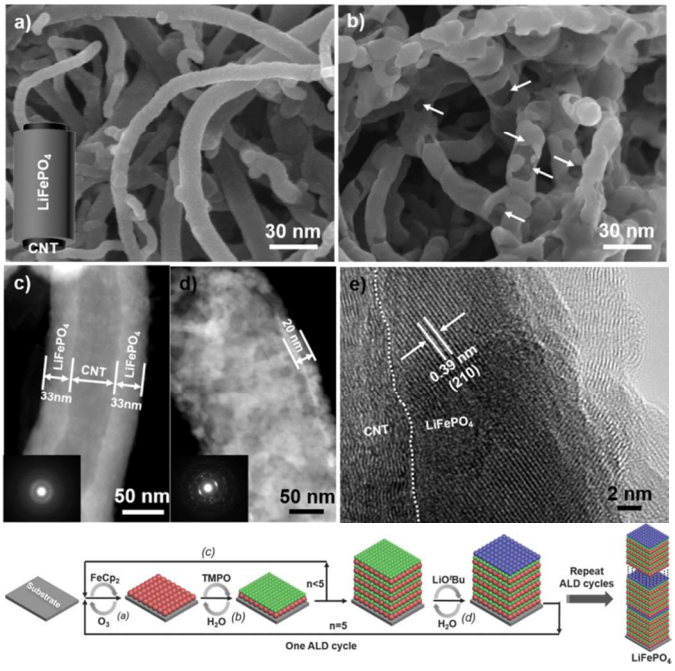

Fig. 6. SEM images of (a) as-prepared CNTs/$LiFePO_4$ and (b) annealed CNTs/$LiFePO_4$; scanning transmission electron microscopy images of: (c) as-prepared CNTs/$LiFePO_4$ and (d) annealed CNTs/$LiFePO_4$; (e) HRTEM image of the annealed CNTs/$LiFePO_4$. (f) schematic illustration showing the ALD principle for synthesis of $LiFePO_4$. Reproduced with permission from ref. 105. Copyright 2014, WILEY-VCH Verlag GmbH & Co. KGaA..

In addition to the above fundamental issues, in practical application, another big issue for lithium iron phosphate is related to the tap density. The large-scale industrial application of lithium ion batteries in electric vehicles not only requires a high specific capacity, but also a high tap density of $LiFePO_4$ which means a high volumetric energy density.[106,107] To meet the requirement of high tap density but maintain all the merits of nanosized materials, porous $LiFePO_4$ microspheres with interconnected open pores are advantageous because it can reduce the diffusion length of lithium ions, facilitating fast lithium ions diffusion.[108-110] Carbon coated $LiFePO_4$ microspheres with high tap densities can be synthesized and produced by coprecipitation, hydrothermal and solvothermal methods. The fundamental understanding of the seed nucleation, growth, precipitation and some other factors (e.g. chemical potentials, the choice of solvents and surfactant addition) as well as the development of a simple, feasible and low-cost synthetic route are still critical for the future of $LiFePO_4$.[111,112] Nanosized $LiFePO_4$, generally synthesized by low-temperature solution routes, is susceptible to the presence of some defects due to the turbostratic stacking of the layers, which leads to perturbation of the lattice and localized charge at the external surface and the 1D channels limiting lithium ion diffusion. In contrast, large-sized crystals with a less disordered arrangement allow undisturbed paths for lithium ion diffusion. The delithiation process is considered to occur near the surface in a large $LiFePO_4$ crystal, however, it is preferable to take place at the core of a small crystal.[113] In addition, Large $LiFePO_4$ particles with high tap densities seem to exhibit a higher degree of electrochemical reversibility. Previous studies indicate some difference in the delithiation behavior between large and small single crystal.[114,115] Based on the above discussion, it is critical to optimize the synthesis conditions to produce well-order $LiFePO_4$ crystals with suitable size (not solely focusing on nanosized crystals), high tap density, few defects and high reversibility.

2.4. Element doping

In addition to carbon coating and morphology/size control strategies, doping is considered to be another significant method to enhance the intrinsic electronic/ionic conductivity of $LiFePO_4$. Especially considering the limited factor for the rate performance due to the poor lithium ion diffusion, substitution of a small amount of Li^+, Fe^{2+} or O^{2-} by other ions is expected to enhance the charge/discharge property at high current densities. Although the role of doping in $LiFePO_4$ is still unclear and under debate, doped $LiFePO_4$ indeed exhibits improved electrochemical performance in numerous reports.

Lithium site doping. The first work about Li site doping was reported by Chung et al. that a significant increase in $LiFePO_4$ electronic conductivity by around 8 orders of magnitude was achieved to reach 10^{-2} S cm^{-1} with low amount of dopant (Mg, Zr, and Nb, no more than 1at.% at Li M1 site).[116] The dramatic increase in conductivity was later attributed to carbon coating and the metallic iron phosphides/carbophosphides on the $LiFePO_4$ surface during the solid state reaction process at high temperatures (above 700 °C).[117,118] Since then, the possibility and practical role of Li site doping has aroused enormous research interest.

From the conventional wisdom, lithium ions diffuse along 1D tunnels in LiFePO4 and the presence of immobile dopants at the Li site certainly impede lithium ion diffusion, which will result in a low rate performance for $LiFePO_4$. Nazar recently revisited this topic by using neutron and X-ray diffraction for aliovalent cation doped $LiFePO_4$ with Zr, Nb and Cr doping elements.[119] The result confirms that these dopants indeed exist on Li M1 sites with ~3 atom% substitution after a solid-state reaction at 600 °C. However, these dopants cannot significantly affect lithium ion diffusion in $LiFePO_4$ because lithium ion diffusion channels only increase 0.3% by these dopants. Instead, these immobile dopants resided within lithium ion channels certainly will hinder lithium ion diffusion, resulting in lower rate performance. Nevertheless, some experimental reports indicate that Li site doping indeed enhance the rate performance of $LiFePO_4$.[120,121] So far, the true role and effects of Li doping for $LiFePO_4$ electrochemical performance has still not been ascertained and remains controversial.

Iron site doping. In comparison to Li site doping, more researchers performed substitution (aliovalent and isovalent) at the Fe (M2) site. Similar to the debates at Li site doping, the feasibility and roles of Fe site doping, especially aliovalent doping, is still under debate. With atomistic simulation method, Islam et al. previously suggest that only divalent metal elements can be doped in $LiFePO_4$ lattice but aliovalent doping is not successful.[122] However, many publications report the improved electrochemical performance of $LiFePO_4$ with aliovalent doping (e.g. Mo^{6+}, Ti^{4+}, V^{5+}, Nb^{5+}).[123-126] From these reported studies, aliovalent doping seems to be feasible and its beneficial role in $LiFePO_4$ electrochemical performance indeed exist. The remaining question is what exactly contributes to this improvement, which has been the research focus for doped $LiFePO_4$.

Among those aliovalent doping elements, vanadium has become one of the most interesting dopants in recent years due to its various oxidation states and coordination chemistry. Vanadium also can form electrochemically active phases (e.g. $Li_3V_2(PO_4)_3$, $LiVOPO_4$ and V_xO_y) and avoid inactive impurity substances in lithium ion batteries. Therefore, some recent works selected vanadium as a model dopant to investigate why aliovalent doping in Fe site can increase the rate of lithium removal/insertion in $LiFePO_4$.[127-129] X-ray diffraction indicates that vanadium doped $LiFePO_4$ at Fe site can reduce the lattice mismatch between Li-rich and Li-poor phases. It also increases the composition width of the single phase (solid solution range), which is beneficial for the fast charge/discharge

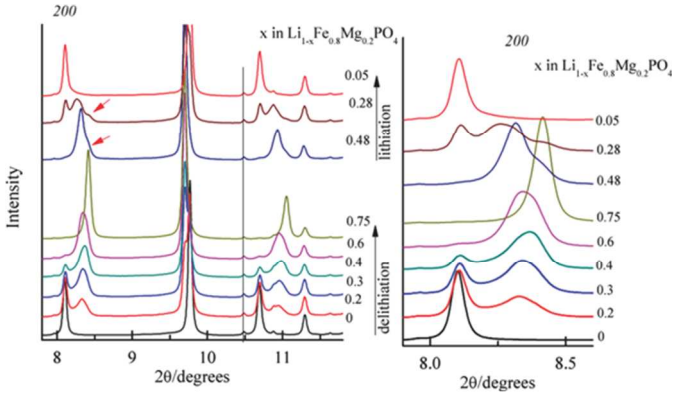

Fig. 7. High-resolution XRD patterns of $LiMg_{0.2}Fe_{0.8}PO_4$ at different states of charge/discharge. Upon lithiation to x = 0.48, two phases are observed. One is the lithium-poor phase (a hump as shown by the arrow) and the other is the intermediate phase. Reproduced with permission from ref. 138. Copyright 2014, WILEY-VCH Verlag GmbH & Co. KGaA..

ability. In addition, the V-doped $LiFePO_4$ show a lower single-phase transformation temperature.[130] Combining X-ray with neutron powder diffraction methods, Whittingham's group recently confirms that the doped alivalent vanadium indeed occupy Fe sites, but some Fe exist at Li sites, which increase the unit cell volume. [131] Similar to the previous report, this aliovalent doping may reduce the miscibility gap and solid solution formation temperature, which contributes to high rate performance. However, this V doping and some Fe resided at Li sites also significantly decrease the capacity of $LiFePO_4$ at moderate temperature. Therefore, the control of proper doping at preferable sites is important for the overall $LiFePO_4$ performance improvement.

In terms of doping process, the element doping involves many factors, including temperature, time, precursors and the $LiFePO_4$ itself. In general, a low ratio of aliovalent ions doping (less than 10 mol%) at Fe site can be achieved by conventional solid state methods, but a higher degree of doping needs novel synthetic routes. With microwave-assisted synthesis process, Harrison recently reported an aliovalent doping with up to 20% V substitution at Fe sites. [132] A temperature dependence of V doping in $LiFePO_4$ was also confirmed. Nevertheless, further studies and optimization of doping experimental parameters are still needed.

Compared with aliovalent doping, isovalent substitution is more normal in nature for $LiFePO_4$, and many divalent cations (e.g. Mn, Co, Ni, and Mg) were doped at Fe site with a high doping degree, showing enhanced electrochemical performance.[133-136] Among of the isovalent cations, Mg^{2+} doping is most often reported to improve the electrochemical kinetics of $LiFePO_4$. From the first-principles density-functional theory, Mg doping prefers to reside at Fe site rather than Li site, leading to high lithium ion diffusion.[137] By using X-ray diffraction for a partially (de)lithiated $LiMg_{0.2}Fe_{0.8}PO_4$ sample, a recent study indicates the existence of stable equilibrium intermediate phases (Fig. 7).[138] As a result, the Mg doped $LiFePO_4$ may undergo single-phase process during lithiation/delithiation process, which may play a significant role in improving the electrochemical performance of Mg doped $LiFePO_4$. In addition, the formation energies and the cell volumes decreased gradually with the increase of Mg concentration in Mg doped $LiFePO_4$, which also enhance lithium ion diffusion rate in $LiFePO_4$.[137]

Isovalent Mg doping at Fe sites can enhance the electronic conductivity and electrochemical activity for $LiFePO_4$. However, that is not the case if the isovalent Mg doping occurs at Li sites. Mg doped $LiFePO_4$ is size-dependent in term of electrochemical

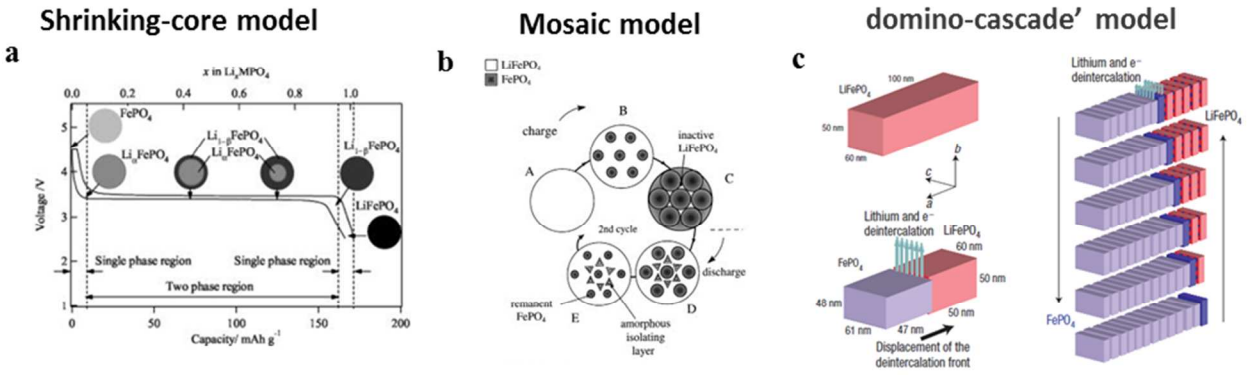

Fig. 8. Several classic two-phase models for $LiFePO_4$. (a) Shrinking-core model, reproduced with permission from ref. 144. Copyright 2005, The Electrochemical Society. (b) Mosaic model, reproduced with permission of ref. 148. Copyright 2001, Elsevier. (c) Domino-cascade model, reproduced with permission of ref. 145. Copyright 2008, Nature Publishing Group.

Table 1. Two-phase models in single-particle $LiFePO_4$ system

Mechanism	Sample size/morphology	Characterization tools	Experimental method	refs
Core-shell	Micrometric particles	X-ray diffraction	Chemical/electrochemical delithiation	1
Shrinking-Core	100-200 nm nanoparticles	Mathematical model	Electrochemical delithiation	18
Radial model	140 nm nanoparticles	High-Resolution Electron Energy Loss Spectroscopy	Electrochemical delithiation	10
Spinodal model	100 nm nanoparticles	Raman and High-resolution Transmission Electron Microscopy	Electrochemical delithiation	146,147
Mosaic model	Solid state route	Neutron powder diffraction	Electrochemical delithiation	148
Domino-cascade model	100 nm nanoparticles	XRD and HRTEM	Electrochemical delithiation	145
Two-phase coexistence	Micrometric LFP particle	In operando Transmission X-ray Microscopy	Electrochemical delithiation	159
Two-phase coexistence	Micrometric single crystals	Transmission X-ray Microscopy	Chemical delithiation	157

performance.[139] Compared with Fe site doping, Mg doped at Li site exhibit a low capacity and poor electrochemical kinetic due to the block effect by Mg on the lithium ion diffusion path. Interestingly, this adverse effect may be diminished after long-term electrochemical cycles, which may be due to the gradual ion exchange between Mg ions and Li ions.

In addition to the above Li and Fe site doping, anion doping at O site was also reported to improve the electrochemical performance such as cycle and rate capability. These doped anions include Cl, F and Na.[140,141] However, compared to the extensively studied Fe and Li doping, O site doping has been less studied and seldom used. There are limited references and resource available. Therefore, no detailed discussion about this topic was presented in this review.

3. Delithiation and lithiation mechanism

Understanding the phase transformation mechanism and the lithium intercalation pathway in $LiFePO_4$ is of crucial importance because the intercalation kinetics directly determines the capacity, rate performance and columbic efficiency. In terms of phase transition mechanism, it is generally accepted that $LiFePO_4$ undergoes a typical first-order phase transformation, with nucleation and growth of the second phase during the lithium extraction/insertion process, leading to a two-phase equilibrium composed of a Li-poor Li_xFePO_4 phase and a Li rich $Li_{1-y}FePO_4$ phase, which gives a stable voltage plateau at ~3.5 V.[142] The unit-cell volumes of both phases remain nearly constant, with the unit cell volumes of two phases varying by only $\Delta V = 6.5\%$.[143] The small volume change during the phase transformation contributes to the unique advantages of LiFePO4, that is superior structural stability and safety, making it an ideal battery material for electric vehicle applications. Although many studies support the two-phase mechanism of $LiFePO_4/FePO_4$, the specific model still remains controversial, including core-shell, [1,144] domino cascade[145], spinodal decomposition [146,147], and mosaic mode [148] etc (Fig. 8, Table 1). Because the delithiation/lithiation kinetics and phase compositions strongly depends on the particle size, morphology and physical properties of the studied $LiFePO_4$ material, the above disagreement and even conflicting models may be attributed to the specific experimental conditions.

In recent years, with the advancement of microscopic and spectroscopic experimental techniques, a solid solution reaction and intermediate phase have been detected in $LiFePO_4$,[149,150] which also provides another possible phase transformation mechanism for $LiFePO_4$. In general, under a typical solid solution reaction for most materials, the lattice parameters and unit-cell volumes change continuously during the phase transformation process. As in the case of $LiFePO_4$, the solid-solution process and possible intermediate phase have been detected at different extreme experimental conditions such as very tiny particle size (tens of nanometers) or ultra-high charging rate (over 10C) via some *in situ* or *in operando* characterization methods. [151-152]

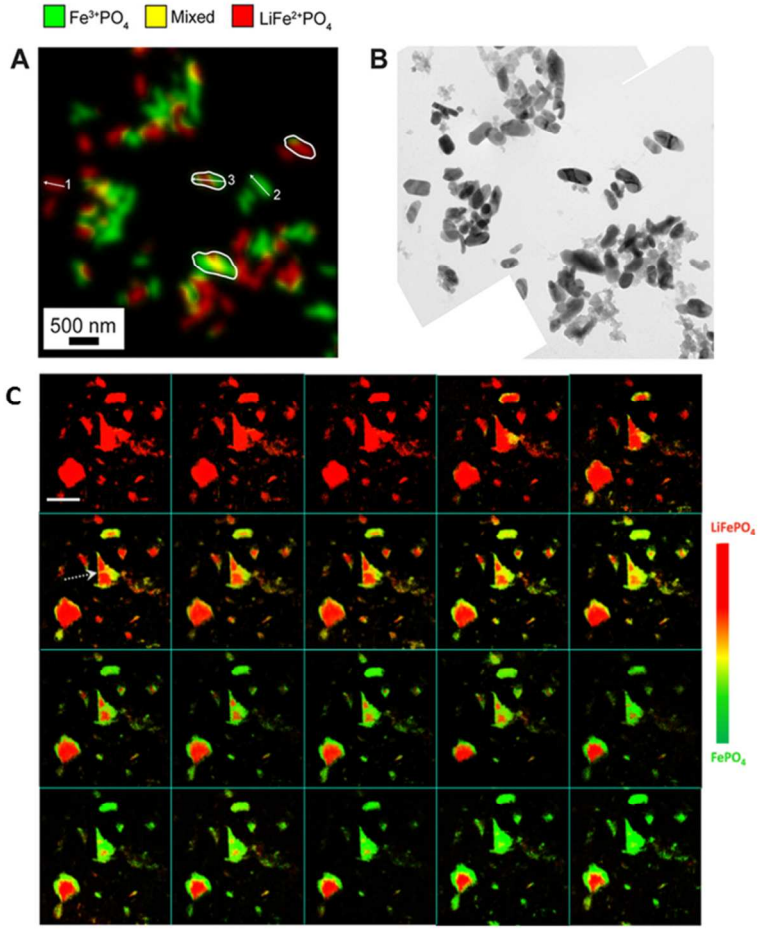

Fig. 9. X-ray chemical mapping of two-phase coexistence in inter-particle (A, soft x-ray imaging of partially charged $LiFePO_4$, B, the corresponding TEM image, an ex-*situ* experiment) and intra-particle (C, *in operando* hard X-ray imaging experiment). The dashed arrows reveal cracks formation in some individual particles in C. Scale bar is 10 μm in C. Reproduced with permission from ref. 158 and 159. Copyright 2013 American Chemical Society (a,b) and 2014 Nature Publishing Group (c).

In addition, the recent research interest on $LiFePO_4$ phase transformation mechanism has been extended from a single-particle to a multi-particle system as well as the entire electrode behaviour, [153-154]. In the case of real $LiFePO_4$ electrodes, there is an assembly of a large amount of active $LiFePO_4$ particles with possible differences in inhomogeneity, thickness and porosity. In this section, we will overview some recent understanding and findings on this hotly debated subject of the $LiFePO_4$ phase transformation mechanism.

3.1. Two phase coexistence

The well-known two phase mechanism in $LiFePO_4$ has two explanations, that is, intra-particle and inter-particle two phase coexistence. Some studies suggest that the two-phase coexistence only occurs in the inter-particle system, that is to say, all the individual $LiFePO_4$ particles are either completely delithiated ($FePO_4$) or lithiated ($LiFePO_4$).[155,156] This explanation has been supported by recent *ex situ* work via Transmission Electron Microscopy (TEM) and X-ray Microscopy (soft and hard X-ray technology).[157,158] However, this two-phase coexistence may change with particle size, morphology and electrochemical testing condition (fast or slow charging rate, static or dynamic, etc). Recent work using hard x-ray microscopy to track $LiFePO_4$ phase transformation under *in operando* condition reveals two-phase coexistence in individual microsized $LiFePO_4$.[159] The microscale sized $LiFePO_4$ is not robust, so the large mismatch between two end members may lead to energy relaxation, revealing by the formation of cracks or structural dislocations but no driving the fast phase transformation. The weak driving force only allows boundary displacement preferring to occur at the surface-near sites, resulting in the two-phase coexistence in the individual large particles.[160-161] In contrast, as for nanosized $LiFePO_4$, the large mismatch and local constraints between the two end members drive fast boundary displacement, allowing the fast phase transformation reaction. As a result, the nanosized $LiFePO_4$ is more susceptible to exhibit either full delithiation ($FePO_4$) or fully lithiation ($LiFePO_4$). Therefore, the size effect plays an important role in the intra-particle delithiation mechanism for $LiFePO_4$ (Fig. 9).[159]

3.2. Solid-solution mechanism

Although the two-phase mechanism had been widely accepted and the presence of the two-phase transformation in $LiFePO_4$ is generally considered to limit its fast charging performance, in practice, $LiFePO_4$ batteries have been successfully commercialized and applied in electric vehicles, demonstrating high rate performance. The contradiction between the theoretically low ion diffusion capability and practically high rate capability pushes us to revisit the two-phase mechanism in $LiFePO_4$. Indeed, some previous theoretical research suggests that the miscibility gap between two end members may decrease and even disappear, but most of the assumption are

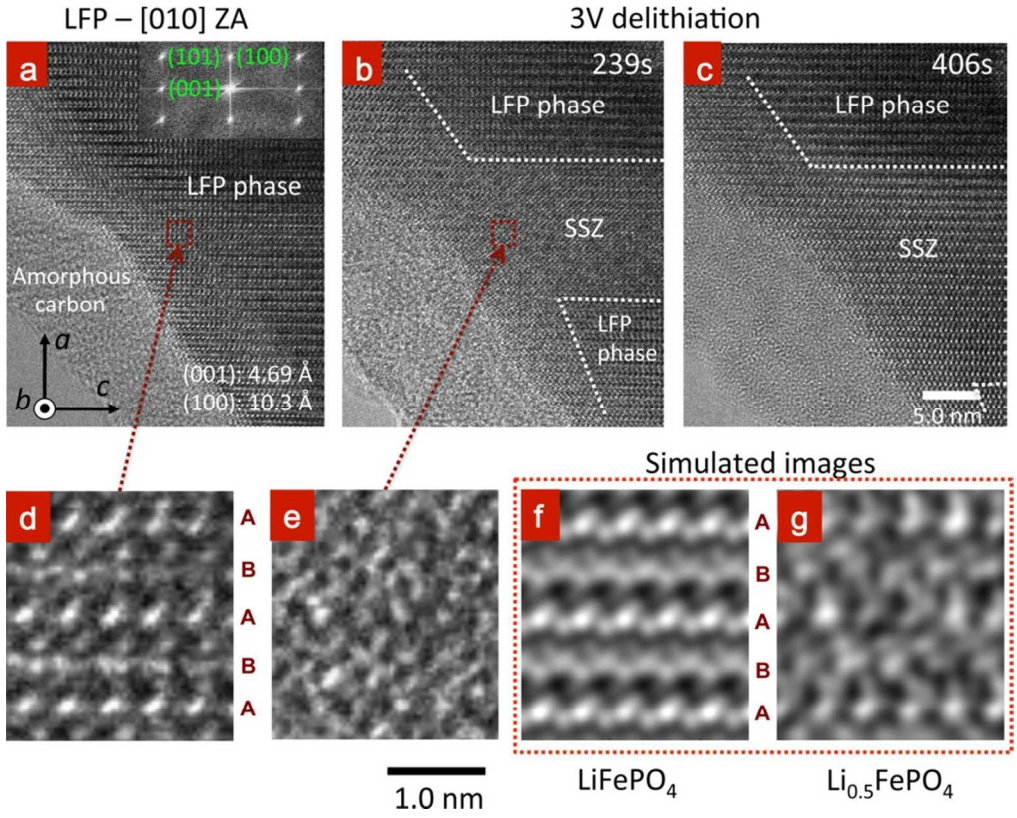

Fig. 10. *In Situ* TEM study of the delithiation process of a $LiFePO_4$ crystal viewed from [010] axis (a–c). (a) The $LiFePO_4$ showing a clear crystal structure before voltage applied. (b) A clear solid solution zone (SSZ)and a directional boundary propagation were observed at 239 s. (c) the images of the SSZ and boundary evolution at 406 s. (d,e) The magnified images of the selected regions in (a,b), respectively. The simulated TEM images of (f) $LiFePO_4$ and (g) $Li_{0.5}FePO_4$. Reproduced with permission from ref. 175. Copyright 2014 American Chemical Society.

only effective under extreme conditions such as using extremely small particles (below 15 nm)[162] or high temperatures (~ 350 °C),[163] which cannot completely explain the high rate performance for true $LiFePO_4$ batteries under practical working conditions (room temperature, hundreds of nanoscales or microscale). As a result, a nonequilibrium solid solution may occur and play a critical role in the observed high rate capability of $LiFePO_4$ electrodes. In recent years, with the advancement of characterization tools and use of *in situ* or *in operando* methods, an increasing amount of experimental evidence validates this assumption.

Based on some theoretical calculations such as first-principles and phase-field modeling, a solid-solution mechanism was previously proposed,[164,165] which suggest the phase transformation between $LiFePO_4$ and $FePO_4$ may undergo a single-phase, not two-phase mechanism. Recent research suggests that the phase separation is able to be suppressed in the nominally two-phase region, especially for nanosized particle at high rates. This was supported by experimental results, as a long-range lithium-ordered $Li_{0.5}FePO_4$ phase in half delithiated $LiFePO_4$ single-crystalline nanowires was shown with TEM.[166] A continuous shift of the diffraction peaks was also shown during lithium insertion/extraction process for $LiFePO_4$ nanoparticle (40 nm) at room temperature.[167] These experimental findings obviously support the above assumption.

Since the realization of the solid solution phases, there arises another debate about the width, form, and role of a solid solution zone during battery charging and discharging. Although the solid solution mechanism has been confirmed, many reported experimental results and conclusion are inconsistent, including an atomically sharp interface,[138] a 4 nm disordered interface,[160,169] and a long-range ordered structure in partially delithiated $LiFePO_4$.[170,171] For example, for this staging structure (a pronounced long-range order), a recent study indicates the size-dependent behavior. As to the small crystals, staging exists in the whole particle with a decrease of order from center to the surface. For the larger crystal, an intermediate phase appears between $LiFePO_4$ and $FePO_4$ and the staging interfacial width changes little with size increase.[172] In addition to the size-dependency, the solid-solution phase transformation in $LiFePO_4$ is also found to be rate-dependent. At high rates such as over 10C, the solubility limits in both phases increase dramatically, leading to a fraction of the electrode material to follow a single phase transformation path, bypassing the first-order phase transition.[173] Obviously, the topic continues to be debated and more fundamental studies and direct experimental evidence is needed.

The convincing evidence for the solid-solution mechanism is a direct characterization of this solid solution zone under *in situ* or *in operando* condition is needed to provide temporal and spatial precision. Previous theoretical calculation show that this solid solution zone is thermodynamically metastable.[174] Using *in situ* high-resolution TEM, Niu et al recently observed a disordered Li-sublattice solid solution zone (10−25 nm × 20−40 nm in size). Different from the sharp interface in other *ex-situ* studies, the observed wide solid solution zone shows no

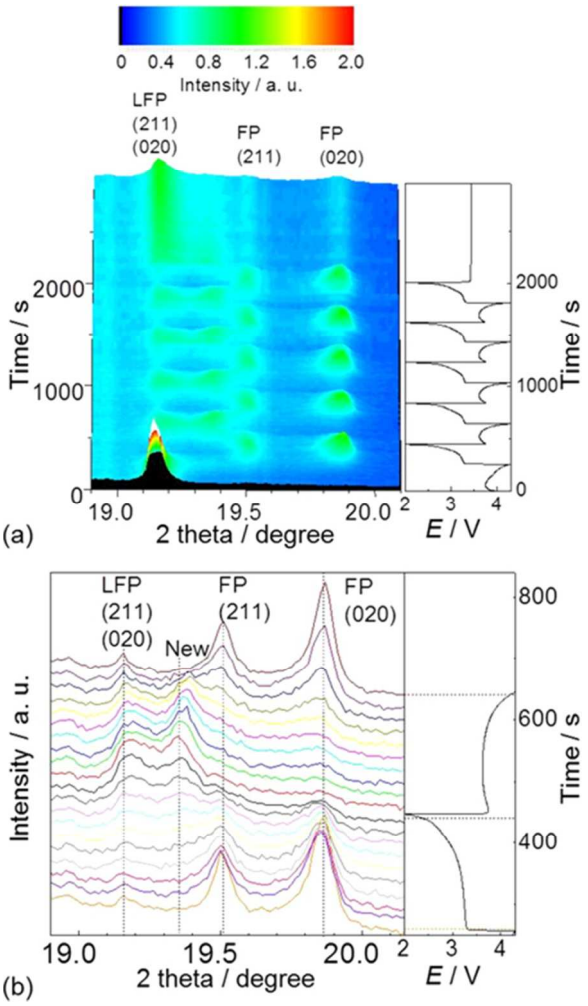

Fig. 11. *In situ* synchrotron XRD study of $LiFePO_4$ under electrochemical cycles. (a) Time-resolved XRD patterns for $LiFePO_4$ during charge–discharge cycles at 10C rate. (b) Detailed XRD patterns during the first discharge and second charge cycles. A new peak at 19.35° was formed during cycling. Reproduced with permission from ref. 179. Copyright 2013 American Chemical Society.

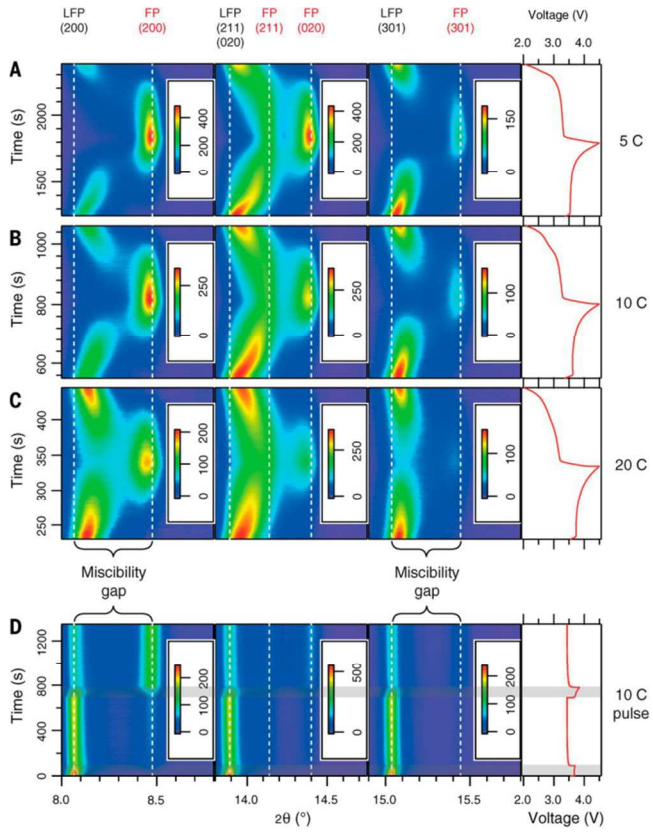

Fig. 12 *In situ* XRD study of $LiFePO_4$ under different electrochemical cycles. (A to C) patterns of the second galvanostatic cycle at 5, 10, and 20 C, respectively. (D) patterns of the evolution of the charge-relax experiment, where a 10 C current is applied for 90 s followed by an open-circuit relaxation of 10 min. Reproduced with permission from ref. 180. Copyright 2014, the American Association for the Advancement of Science (AAAS).

dislocations, which is considered to contribute to the high rate performance of $LiFePO_4$. In addition, it also suggests that this disordered solid solution zone could dominate the phase transformation process even at high charging rates. This dynamic observation provides a more accurate understanding the solid solution zone (Fig. 10). [175]

Further experimental evidence was also obtained via *in-situ* synchrotron x-ray study. Because of the high sensitivity, time resolution, and accuracy,[176-178] synchrotron x-ray diffraction is the most suitable technique to detect the possible intermediate phase under charging and discharging of $LiFePO_4$. With the *in operando* XRD technique, Orikasa et al [179] tracked the phase transformation process and found a metastable crystal phase in fast-charging microsized $LiFePO_4$, in addition to the thermodynamically stable $LiFePO_4$ and $FePO_4$ phases (Fig. 11). Also, it was found that this metastable phase has a short life time (a couple of minutes), as it diminishes under opencircuit conditions. This metastable Li_xFePO_4 (x = 0.6−0.75) only appears at high charging rates, and is absent at slow-charging rates in the $LiFePO_4$ electrode. Therefore, it is suggested that at high rates, the phase transformation in $LiFePO_4$ may pass through the metastable phase, which decreases the nucleation energy and thus leads to a higher rate performance for the $LiFePO_4$. Another one of the latest *in situ* XRD studies captured the metastable solid solution phase in fast charging nanosized $LiFePO_4$ (Fig. 12).[180] Different from the intermediate Li_xFePO_4 (x=0.6-0.75) phase at high rates in the microsized samples, the studies at nanosized $LiFePO_4$ demonstrate the continuous solid solution phase has a wide composition, Li_xFePO_4 (0<x<1). This is composed of the entire range between the two end members of $LiFePO_4$ and $FePO_4$ at high rates. It suggests that nanosized $LiFePO_4$ may undergo continuous structural change without the phase boundary movement and nucleation step, which also helps explain the high rate performance of $LiFePO_4$.

Furthermore, the (de)lithiation mechanism and solid solution formation is also related to the type of olivine lithium phosphate. A typical example is lithium manganese iron phosphate (LMFP), a very promising cathode material with a higher working voltage and similar structural stability.[181,182] Recently, *in operando* synchrotron XRD indicated that, in contrast to $LiFePO_4$, nano-LMFP exhibits a continuous solid solution process, which can be observed at a wide composition range. The dominated metastable solid solution process occurring at LMFP can explain the higher rate capacity than $LiFePO_4$ with comparable particle sizes, in spite of a larger volume misfit (11.6 for $LiMnPO_4$, 6.5% for $LiFePO_4$).[183]

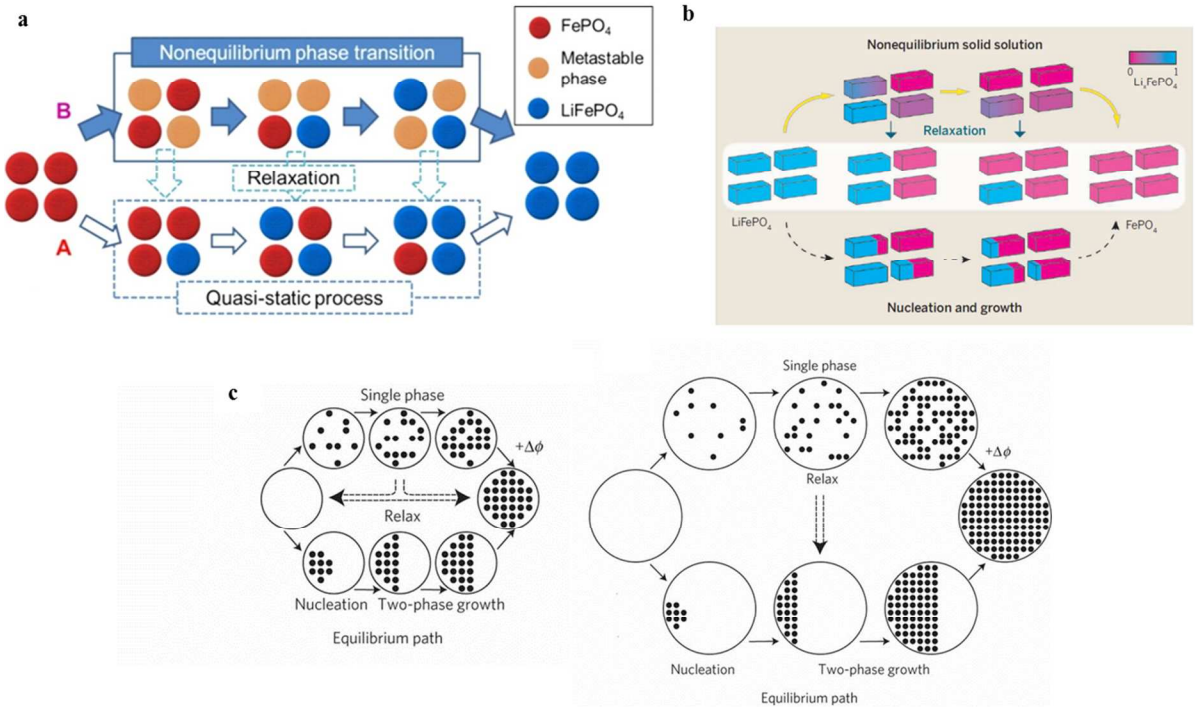

Fig. 13. Non-equilibrium phase transition via a metastable phase (a), solid-solution (b) and single phase model (c). Reproduced with permission from ref. 179, 180 and 19. Copyright 2013 American Chemical Society (a), 2014 the American Association for the Advancement of Science and 2011 Nature Publishing Group, respectively.

Table 2. Solid-solution mechanism confirmed by a variety of experimental studies

Sample	Characterization tools	Experimental method	Driven force	refs
500 nm particles	XRD	Chemical delithiation with NO_2BF_4	Temperature driven solid solution, Li_xFePO_4 ($0\le x\le 1$) at 450°C	165
NA	NA	Phase-field model	Current density	20
100 nm nanoparticle	NA	Density functional theory calculations	Low overpotential at non-equiibrium path	19
Micrometric particle	Time-resolved XRD	Electrochemical (de)lithaition	High (de)charge rates (10C), a metastable $Li_{0.6\text{-}0.75}FePO_4$ solid-solution phase	179
100 nm $LiMn_{0.4}Fe_{0.6}PO_4$ particles	In operando synchrotron XRD	Electrochemical (de)lithiation	Olivine composition, the metastable solid solution covering a remarkable wide compositional range	183
10-180 nm nanoparticles	In situ synchrotron XRD	Electrochemical (de)lithaition	High cycling rates, the solid solution phase, Li_xFePO_4 ($0<x<1$) covering the entire phase composition	180

A similar report from Whittingham's group also indicates that Li(Mg, Mn, Fe)PO_4 undergoes a one-phase (de)lithiation mechanism. Mg substitution in the mixed olivine, $LiFe_{0.6}Mn_{0.4}PO_4$, reduces the lattice misfit between the two end-member phases. This smaller lattice mismatch and the interactive forces (Mn, Fe and Mg) result in a one-phase (de)lithiation mechanism.[184]

The (de)lithiation mechanism is also related to $LiFePO_4$ structure. Recently, a novel non-olivine $LiFePO_4$ with an alluaudite structure was successfully developed.[185] In contrast to the two-phase reaction in olivine $LiFePO_4$, the alluaudite $LiFePO_4$ showed fundamentally different electrochemical behavior. In spite of the similar Fe^{2+}/Fe^{3+} redox reaction, the alluaudite $LiFePO_4$ showed a one-phase reaction mechanism, allowing fast lithium ion diffusion. The fast charging property is attributed to the unique structure of the alluaudite. An alluaudite compound has a formula $X(1)X(2)M(1)M(2)_2(PO_4)_3$ and the structure contains edge sharing $M(2)O_6$ octahedra chains, connected by distorted $M(1)O_6$ octahedra. X(1) and Li in the targeted structure occupies in X(2) site, and Fe occupies M(1) and M(2) sites. Tetrahedral PO_4 units connect the chains, and X cations reside in tunnels along the c-axis providing possible diffusion pathways. Although this novel structured $LiFePO_4$ enhance the fast charging performance via a one-phase mechanism, many issues related to the alluaudite structure are still unclear such as the thermal stability and electronic conductivity. Also, only around 0.8 lithium ions could be delithiated and reversed back in the one-phase

reaction. The specific capacity and cycle performance are unsatisfied. Further studies are still needed.

In addition to the proposed two-phase and solid-solution mechanisms, a mixed mechanism has also recently been suggested. With *in operando* synchrotron high-energy X-ray diffraction (XRD), nonequilibrium lithium insertion and extraction from the $LiFePO_4$ cathode was studied. Neither the $LiFePO_4$ phase nor the $FePO_4$ phase maintained a static composition during lithium insertion/extraction.[186] Instead, the $LiFePO_4$ cathode simultaneously experienced both a two-phase reaction mechanism and a dual-phase solid-solution reaction mechanism over the entire range of the flat voltage plateau, with this dual-phase solid-solution behavior being strongly dependent on charge/discharge rates. The proposed dual-phase solid-solution mechanism may explain the remarkable rate capability of $LiFePO_4$ in commercial cells. The similar mechanism was also reported by *in situ* neutron powder diffraction and the simultaneous occurrence of solid solution and two-phase reactions after deep discharge under nonequilibrium conditions was suggested (Fig. 13, Table 2).[187]

3.3. Multi-particle system

Since numerous studies of the (de)lithiation mechanism are based on individual $LiFePO_4$ particles, understanding of the entire electrode behavior is still not clear. This is because the mechanism in a single-particle $LiFePO_4$ system may not necessarily suitable for an entire electrode, considering the issues from thickness, inhomogeneity, porosity and particle overlapping. Recent research has suggested that in an electrode assembly, all $LiFePO_4$ particles are not (de)lithated simultaneously but sequentially via a particle-by particle intercalation pathway.[188] That is to say, in contrast to the "concurrent" mechanism, two-phases coexist in inter-particle at the entire electrode, which is considered be due to the fast inter-particle transport, the quick phase boundary replacement and the decrease of interfacial energy.[189]

The inhomogeneous $LiFePO_4/FePO_4$ phase distribution at entire-electrode scale was confirmed by *ex-situ* Scanning Transmission Electron Microscopy (STEM).[190] At the mesoscale, a core-shell phase distribution with a preferential pathway along porosities was found. At a larger scale, the (de)lithiation process occurs via a "stratum by stratum" pathway from the electrolyte side to the current collector. It is obvious that electrochemical reaction is more favorable to occur at some electrolyte-accessible sites with more porosity, as lithium ion diffusion is one of the main limiting factors. Another study with in situ soft X-ray spectroscopy also indicates

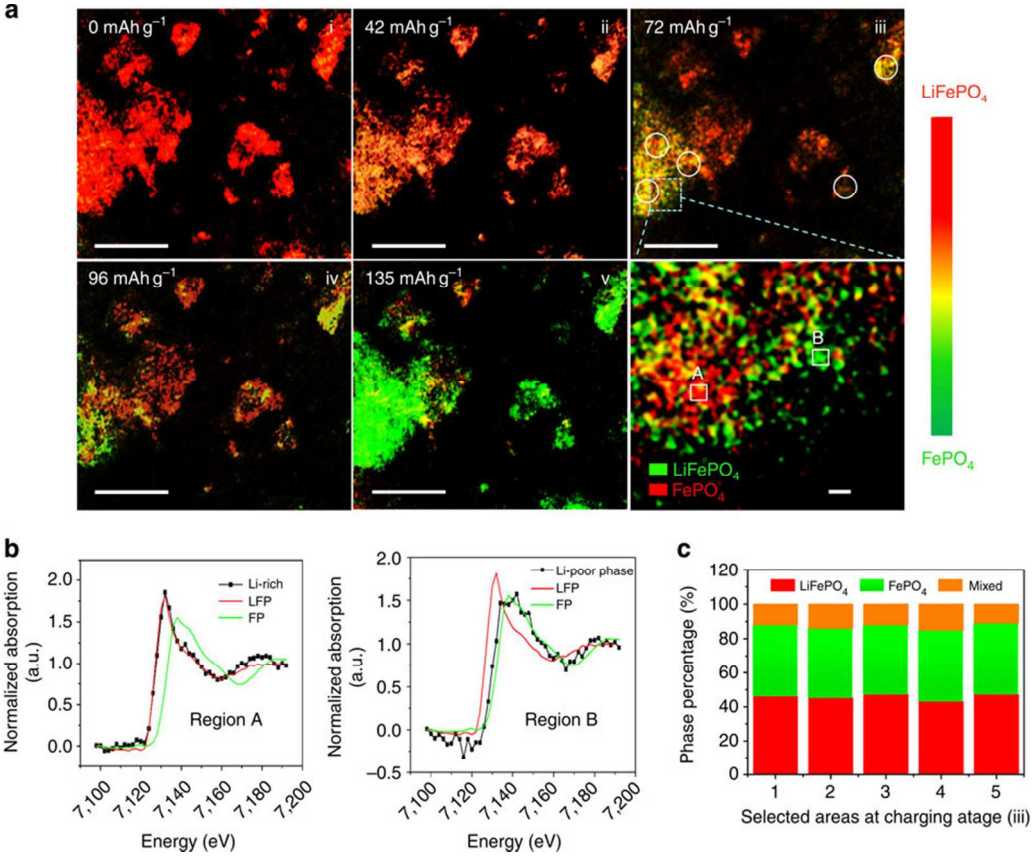

Fig. 14 *In operando* chemical mapping of multi-particle $LiFePO_4$ system at a 5C rate. (a) 2D chemical mapping; (b) XANES at selected regions A and B at charging stage iii; (c) Statistical histograms of phase compositions at five selected regions at charging stage iii. Scale bar: 10 μm for the five 2D maps, 200 nm for the enlarged map. Reproduced with permission from ref. 159. Copyright 2014 Nature Publishing Group.

Table 3. Synchrotron X-ray imaging techniques for $LiFePO_4$ studies

Methods	Energy range	Sample thickness	Spatial resolution	Pressure condition	*In situ* operation	refs
Hard X-ray microscopy	4k-13K eV	Up to micron scale	<30 nm	Ambient	easy	159
Soft X-ray microscopy	200-2K eV	Up to hundreds of micron	<30 nm	Vacuum/half vacuum	difficult	158

that phase transformation starts from the region adjacent to current collectors in a $LiFePO_4$ electrode,[191] confirming the inhomogeneity in $LiFePO_4$ phase transformation.

More direct evidence of the phase transformation comes from a recent *in operando* imaging study. Wang et al tracked the phase transformation evolution on the electrode scale using transmission x-ray microscopy under *in operando* conditions.[159] The unique capability of this *in operando* imaging method is that it can work on a true coin cell without a specialized cell design, therefore, truly revealing the electrochemical process in the $LiFePO_4$ electrode. With this technique, it is suggested that there is a rate-dependent inhomogeneity behavior in a multi-particle $LiFePO_4$ system. At a slow charging rate, a homogeneous phase distribution is found and the entire electrode shows a similar chemical composition, whereas a fast charging rate leads to inhomogeneity and two-phase coexistence in the electrode. The inhomogeneous phase composition only takes place in a fast charging $LiFePO_4$ electrode, which emphasizes the crucial role of electrode architecture in the (de)lithiation process in a multi-particle system, as an electrode structure (thickness, porosity, conductive carbon network, etc) significantly affect the inter-particle intercalation pathway at high rates. This finding motivates more future efforts in optimizing the entire electrode structure to improve rate performance for $LiFePO_4$ (Fig. 14, Table 3).

Understanding of these complex (de)lithiation mechanism has heavily relied on advanced characterization tools. Recent advances in synchrotron X-ray technologies, in particular synchrotron X-ray microscopy, allow to probe large volumes of battery materials at high spatial resolution with accurate chemical/electronic structural information. A new record of 5 nm resolution has recently achieved by soft X-ray ptychography,[192] breaking through the limits of optics (Fig. 15), which will provide more powerful capabilities for elucidating the complex mechanism of battery materials.

4. Surface and interface chemistry

4.1 Surface chemistry-performance improvement

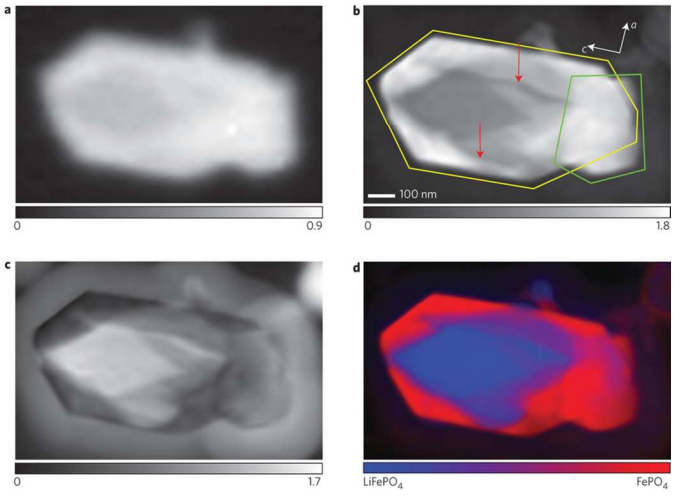

Fig. 15. X-ray microscopy of partially delithiated LiFePO4. a,b, Optical density maps from STXM (a) and ptychography (b) at 710 eV, showing maximum. c, Phase of the ptychographic reconstruction at 709.2 eV, showing maximum relative phase shift between the end members. d, Colourized composition map calculated by principal component analysis absorption contrast between the end members.. Reproduced with permission from ref. 192. Copyright 2014 Nature publishing group.

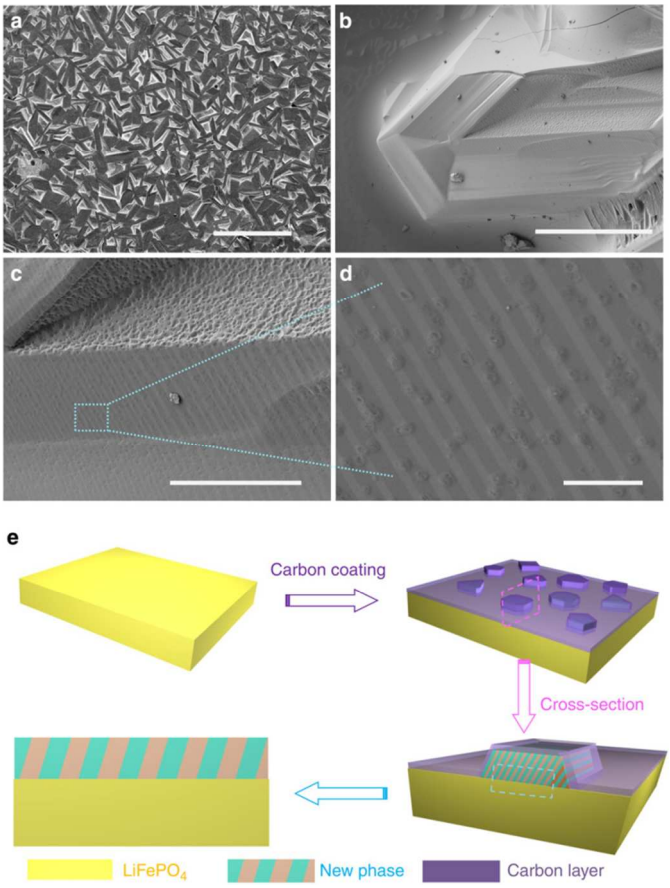

Fig. 16 (a–d) SEM image of surface phase formation on $LiFePO_4$ after carbon coating. (e) Schematic representation of surface phase formation on $LiFePO_4$. Scale bar, 1 mm (a), 500 µm (b), 100 µm (c) and 1 µm (d). Reproduced with permission from ref. 197. Copyright 2014, Nature Publishing Group.

Surface chemistry plays an important role in determining the rate-performance of $LiFePO_4$. Since a $Li_4P_2O_7$-like fast ion-conductive phase was first suggested by Ceder to improve the rate-performance of $LiFePO_4$,[193] surface modification with some stable lithium ion conductors is considered to be one of the strategies to improve lithium ion transport in $LiFePO_4$. For example, by coating novel coralline glassy lithium phosphate onto nano-$LiFePO_4$ particles, it enhances the reversible capacity, cycle performance and rate performance. This highly effective lithium ion conductor increases lithium ion diffusion across the surface (010) and into the $LiFePO_4$ bulk, and improves lithium ion transfer kinetics. In addition, this lithium-including material also provides extra lithium sources to raise the lithium capacity and improves the cycle performance of $LiFePO_4$ electrode.[194] In addition to lithium ion diffusion into $LiFePO_4$, the solid-electrolyte interface also plays an important role in the rate performance of LFP.[195] If the lithium diffusion kinetics at the interface can be improved, a faster charging capability may be achieved allowing even larger sized $LiFePO_4$ (e.g. micron-scale) to exhibit a high rate performance. To enhance lithium diffusivity into the $LiFePO_4$ electrode, with the electrostatic attraction role, Wang et al mixed $LiFePO_4$ with anion absorbents to enhance the delithiation process and the rate performance for $LiFePO_4$.[196] In spite of the enhanced electrochemical performance, the fundamental understanding of

these surface ionic conductors and their true roles are still under debate, as it is always influenced by a carbon coating. Furthermore, these surface ionic conductors may not be very electron conductive and possibly only work at some local sites such as the (010) channel surface. The synthesis and deposition of these surface conductors at particular sites is another challenge.

4.2 Surface chemistry-new phase formation

As a simple and effective method to enhance $LiFePO_4$ conductivity, carbon coating has achieved enormous success and has been widely applied in industrial productions. Nevertheless, due to the strong reducing atmosphere from carbon coating under high temperatures, the surface chemistry change of $LiFePO_4$ is unclear. With a $LiFePO_4$ ingot sample composed of a flat surface, Wang et al recently found the direct evidence of the significant influence of carbon coating on the $LiFePO_4$ surface chemistry. [197] A size-dependent surface phase change was found in $LiFePO_4$ during carbon coating. It was found that, for larger sized $LiFePO_4$, new $Fe_2P_2O_7$ phases with poor conductivity were observed at the ingot surface, as shown in Fig.16. This surface melting and chemistry change occurs under the reducing environment created during carbon coating, resulting in a nonstoichiometric mixture in the molten phase. During the cooling process, the new phase of $Fe_2P_2O_7$ precipitates from the nonstoichiometric molten mixture, accompanied by Li_2O loss. These surface phase changes may even occurs at temperatures as low as 650 ^oC, which is comparable to industrial synthesis temperature for $LiFePO_4$. In contrast, nanosized $LiFePO_4$ shows an extremely high stability. Even carbon coating at temperatures as high as 1000 ^oC, $LiFePO_4$ shows a high purity without any new phase formation. This is attributed to the precipitation rate of carbon atoms on the surface of nanosized $LiFePO_4$ being higher than its diffusion rate. This leads to the rapid formation of a carbon protection layer and accordingly, limits the further interaction between the hydrocarbons and $LiFePO_4$. Therefore, considering the industrial production of large-sized $LiFePO_4$ to improve tap density and volumetric energy density, one has to consider the possible unexpected surface phase change and new phase formation carbon coating.

4.3. Surface chemistry-aging and storage properties

In addition to performance improvements and surface phase changes under carbon coating, most studies have made the correlation between the surface chemistry and $LiFePO_4$'s aging and storage stability.[198-200] As a stable cathode material, previous studies confirm the excellent stability of $LiFePO_4$ in many conventional electrolytes upon electrochemical cycling. [201-203] In addition to the unique structure that restrains oxygen release, as for the (010) facets from which lithium ions preferably transfer, first principle calculations shows a lower surface energy and redox potential (2.95 V) than other facets. This also provides another explanation for the high stability of $LiFePO_4$ during electrochemical cycling.[95] However, in practical storage and long-term electrochemical cycling, the performance fade is still observed; especially at elevated temperatures.[204] The widely accepted reason is the HF formation in moisture-contaminated electrolytes resulting from chemisorbed water and the presence of hydrogen bonds.[205] However, in practical application of lithium-ion batteries, it is hard to completely avoid a very small amount of moisture; in particular the contamination may occur during cell assembly. When $LiFePO_4$ surface is in contact with electrolytes that has a small amount of OH groups, corrosive HF is formed from chemical reaction with the nearby PF6 anions in the electrolyte. [206] As a result, iron dissolution occurs and the $LiFePO_4$'s performance decreases.

Considering iron dissolution and related material stability, studying the aging of $LiFePO_4$ has attracted more and more attention.[207,208] An in-depth structural investigation indicates that when moisture (water) or hydroxyl groups contaminate the electrolytes, iron (II) is oxidized to iron (III) at the surface of $LiFePO_4$ particles, possibly resulting in the formation of electrochemical inactive $LiFePO_4(OH)$ tavorite.[209] The presence of this ferric phase changes the pristine chemical composition and decreases the specific capacity of the $LiFePO_4$. It also affects the cycling and reversible electrochemical behavior due to the inactive ferric surface layer. Furthermore, the transition metal can move to the negative electrode and be reduced to metallic clusters, resulting in the formation of solid electrolyte interphase, capacity loss and serious safety issues.[210]

Wang et al recently presented a direct experimental observation of the surface aging process and iron dissolution in olivine $LiFePO_4$ that was stored in moisture-contaminated electrolyte.[211] Using a $LiFePO_4$ ingot sample with a flat surface as the model material, iron dissolution and surface chemistry changes could be clearly observed. As expected, the iron dissolution is directly related to the $LiFePO_4$ aging process. In addition to the surface chemistry of the $LiFePO_4$ material itself, the study also indicated the direct relationship between the surface aging process and the inhomogeneous surface chemistry (impurity phases). It is well known that some common impurity phases (e.g. Fe_2O_3, Fe_2P, Li_3PO_4, etc.) often exist from the $LiFePO_4$ synthesis process.[212,213] As inactive materials, the presence of these impurity phases not only decreases utilization of active $LiFePO_4$, it also significantly affects the physical, chemical and electrochemical performance of $LiFePO_4$. It was also found that impurities may accelerate the surface aging process of $LiFePO_4$ because an oxidation-reduction reaction occurs at local sites with impurity phases, similar to the metal corrosion mechanism.[214] Iron-rich impurity phases significantly corrode due to the lower corrosion potentials, which inhibit the corrosion of the adjacent $LiFePO_4$ bulk. In contrast, phosphorus-rich impurity phases are more stable due to their higher corrosion potentials, however, these results in the corrosion reaction occurring in the adjacent bulk $LiFePO_4$.[215]

Having elucidated where $LiFePO_4$'s failure originates, strategies to limit surface aging are suggested. The most economic and effective method to protect $LiFePO_4$'s surface is a carbon coating layer. Recent research shows a significant improvement in $LiFePO_4$ surface chemistry stability with a nano-carbon coating, as the carbon surface layer protects $LiFePO_4$ from direct contact with the corrosive medium, effectively restraining the surface corrosion and preserving the initial surface chemistry of $LiFePO_4$, as shown in Fig. 17. [211] This conclusion is clearly confirmed by the Fe K-edge XANES change found during the aging process. After the same surface aging treatment, a clear edge shift in the spectra can be observed on the bare $LiFePO_4$ without a carbon coating due to the oxidation of Fe(II) to Fe(III). In contrast, the iron valence state change is absent in the carbon coated sample, indicating

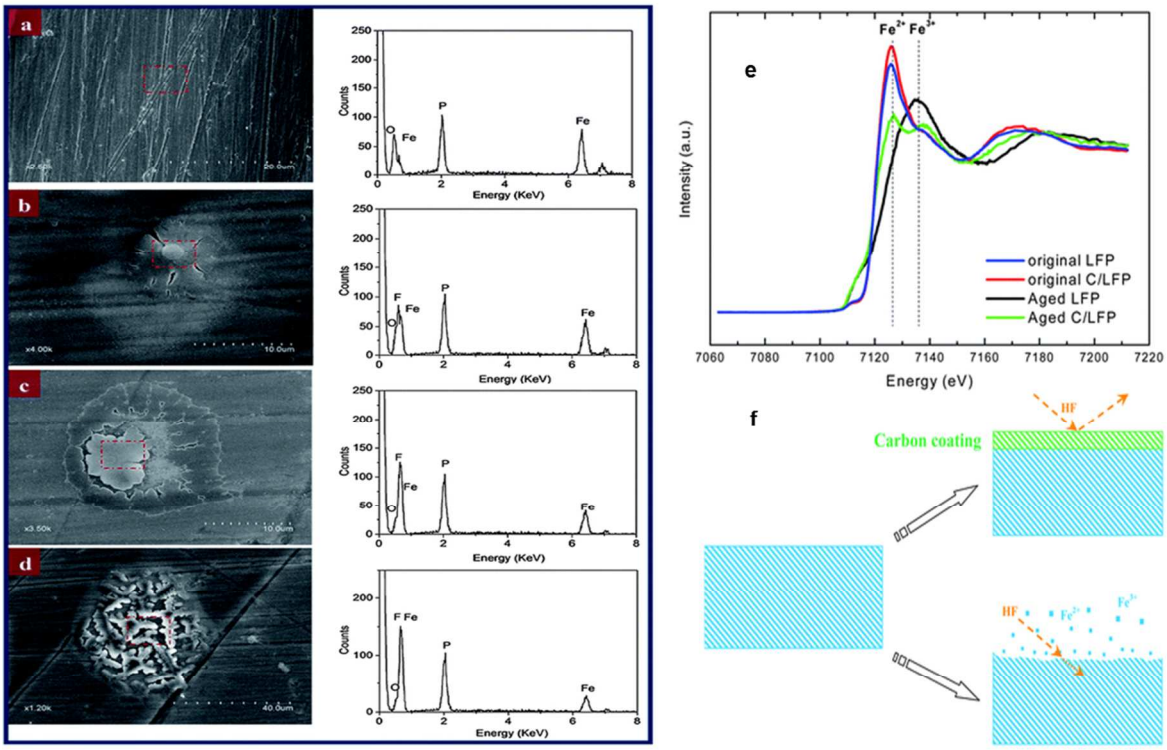

Fig. 17 (a-d) Iron element dissolving on the $LiFePO_4$ surface during the surface aging process at (a) 0 h, (b) 8 h, (c) 24 h and (d) 32 h. (e) Fe K-edge XANES spectra of pristine $LiFePO_4$ and aged LiFePO4 samples. (f) Schematic illustration showing carbon layer protection for surface aging. Reproduced with permission from ref. 211. Copyright 2013, the Royal Society of Chemistry.

the protection role of the carbon coating for $LiFePO_4$'s surface chemistry stability.[211] In spite of the positive protection role of the carbon coating, further surface engineering to improve $LiFePO_4$ stability is still needed because a sole carbon nanolayer may not withstand the long-term electrochemical cycling. Because of the lattice parameter mismatch, there is a coherency strain between the two phases of $LiFePO_4$ and $FePO_4$. As a result, with electrochemical cycling, the stress in the electrode continuously increases, which may lead to the separation of the carbon/$LiFePO_4$ interface. [216] This separation or partial "isolation" of carbon from $LiFePO_4$ will cause the direct exposure of $LiFePO_4$ to the electrolyte, which weakens the carbon layer's protection and surface chemistry stability. In addition, the "uncovered" $LiFePO_4$ also exhibits poorer electronic conductivity. It is well known that in the case of an electrochemical reaction, only both simultaneously electronic and ion accessible sites are electrochemically active. Therefore, the separation of carbon from the $LiFePO_4$ surface will decrease the number of electrochemical triple contact sites, which results in the decrease of the specific capacity and cycle performance. Therefore, further enhancement of the bonding between carbon layer and $LiFePO_4$ is crucial for $LiFePO_4$ surface chemistry stability.

5. Olivine phosphates for Sodium ion batteries

For the demands of low-price and availability, the development of rechargeable batteries for large-scale energy systems using abundant resources and cheap raw materials has become inevitable. Sodium has many similar chemical properties to lithium, and is abundant, inexpensive and environmentally friendly. Thus, sodium-ion batteries are considered to be suitable alternatives to lithium-ion batteries in future large-scale energy storage systems.[217-219] Inspired by the successful commercialization and remarkable electrochemical properties of $LiFePO_4$, the electrochemical and structural study of olivine $NaFePO_4$ has attracted much interest.[220-222] Unfortunately, current olivine $NaFePO_4$ exhibits unsatisfactory electrochemical performance in sodium-ion batteries and faces many challenges.

5.1. Asymmetry electrochemical behavior and phase transformation

One challenge is related to the understanding the complex phase transformation mechanism. Although sharing the same phase structure as olivine $LiFePO_4$, $NaFePO_4$ exhibits a significantly different mechanism in both thermodynamics and reaction kinetics during Na-ion insertion/extraction. The phase transformation process occurring in Na_xFePO_4 does not proceed with a constant composition, therefore, the results and conclusions for lithium-ion batteries may not be directly applied or transferable to sodium-ion batteries. [223]

Different from the one charge/discharge plateaus for $LiFePO_4$, the charge/discharge profile and CV show two plateaus (~2.88 V and ~3.02 V vs. Na/Na^+) when charging but only one plateau for $NaFePO_4$ when discharging.[224-226] It seems that the two potential plateaus are separated by the formation of an intermediate phase ($Na_{\sim 0.7}FePO_4$) during the desodiation process (from $NaFePO_4$ to $FePO_4$), but the three phases ($FePO_4$, $NaFePO_4$, $Na_{\sim 0.7}FePO_4$) appear simultaneously during the sodiation process (from $FePO_4$ to $NaFePO_4$). This asymmetry electrochemical behavior may be related to the larger structural mismatch, in which a 17.58% volume difference is found with

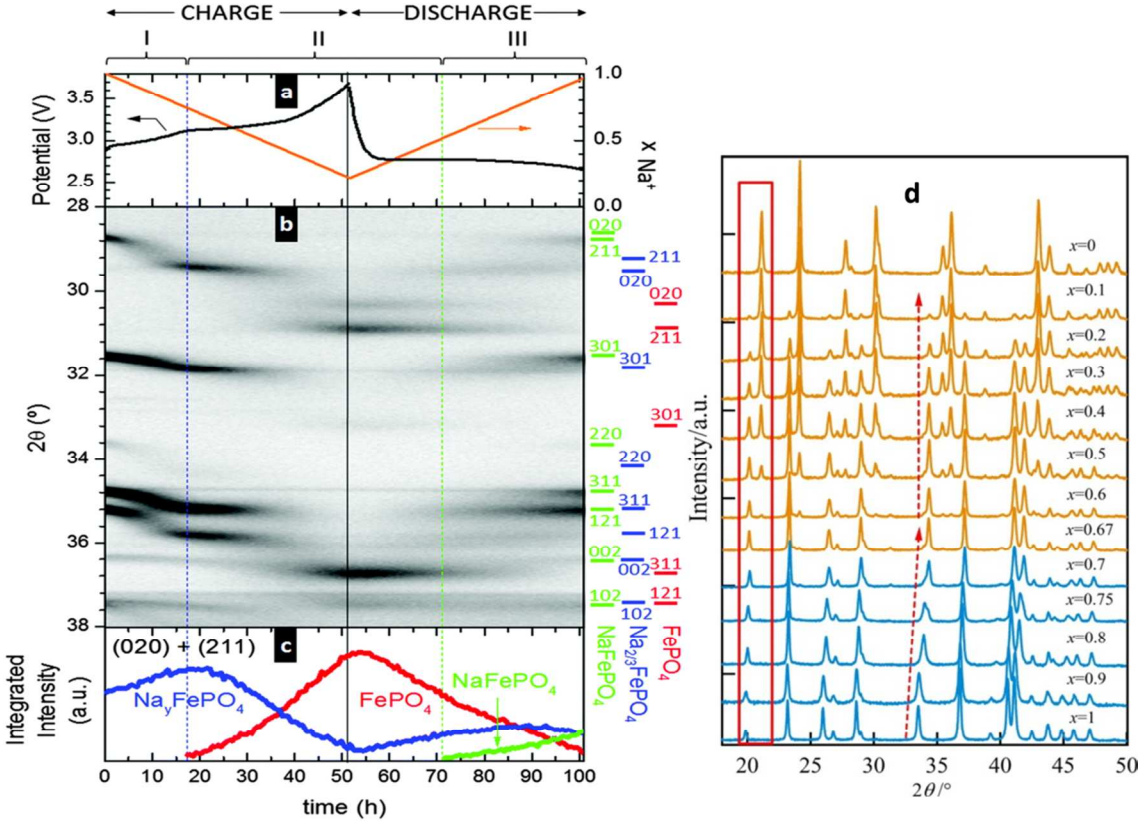

Fig. 18. (a-c) *In situ* XRD of $NaFePO_4$ under the charge/discharge cycles. (b) the detailed XRD patterns at a full cycle (charge and discharge). (c) Summary of the integrated intensity of the (020) and (211) reflections for each of the formed phases.(194) Reproduced with permission from ref. 227. Copyright 2014, the Royal Society of Chemistry. (d) XRD spectra of Na_xFePO_4 as functions of x, a single phase zone ($2/3 < x < 1$), and a mixture of $Na_{2/3}FePO_4$ and $FePO_4$ zone ($x<2/3$). Reproduced with permission from ref. 226. Copyright 2014, the American Chemistry Society.

$FePO_4$/$NaFePO_4$, two times higher than $FePO_4$/$LiFePO_4$.[227] Furthermore, the redox potential gap in $NaFePO_4$ is much larger (3-4 times) than the one in $LiFePO_4$, which also explains the poorer Na ion insertion/extraction kinetics in $NaFePO_4$, in comparison to $LiFePO_4$ (Fig. 18).

More and more experimental results and structural analysis confirm the two-steps desodiation process in $NaFePO_4$. During the first step, sodium is extracted from $NaFePO_4$ through a single homogeneous phase process until the intermediate phase when $Na_{2/3}FePO_4$ forms at the voltage discontinuity (that is, a solid solution process for Na_xFePO_4, $1>x>2/3$). In the second step, sodium extraction occurs in a two-phase process between a Na-rich Na_yFePO_4 phase and a Na-poor $FePO_4$ phase whose composition has been found to vary with overall Na content in the electrode (that is, a two-phase process between $Na_{2/3}FePO_4$ and $FePO_4$). As a result, contrary to the symmetrical biphasic mechanism observed in micrometric $LiFePO_4$, Na extraction occurs in two voltage plateaus separated by an intermediate phase Na_xFePO_4 ($x\sim2/3$), whereas three phases ($FePO_4$, $Na_{2/3}FePO_4$ and $NaFePO_4$) appear simultaneously during Na insertion.[225] The crystal structure of $Na_{2/3}FePO_4$ has been recently studied in details with synchrotron X-ray diffraction and defined as a superstructure due to Na/vacancies and charge ordering.[228,229] The intermediate phase at $x = 2/3$ for Na_xFePO_4 is also much more stable, in comparison to the lithium equivalent. The large cell mismatch (17.58% for $FePO_4$–$NaFePO_4$ compared to 6.9% for the Li counter-parts) enhances the effects of the diffuse interface, which has a higher impact on the Na-ion than Li-ion intercalation chemistry, and therefore a reduced miscibility gap in the overall composition are observed here in micrometric materials.[227] Recently, a detailed understanding of the intermediate phase, $Na_{2/3}FePO_4$, has been reported. With a variety of characterization methods, Boucher et al proposed a three-fold superstructure for the $Na_{2/3}FePO_4$ intermediate phase, with a dense plane being formed by the 2/3 Na and 1/3 vacancy sub-lattice in the intermediate phase, related to the second/third shortest Na-Na distances.[230] This finding introduces a new strategy to develop high-rate olivine cathodes for Na-ion batteries by producing grains with larger (101) surface areas.

Due to the different phase transformation thermodynamics, the reaction kinetics (rate performance) and cycling stability of $NaFePO_4$ were also shown to be much worse than $LiFePO_4$. For example, a specific capacity of 147 mA h g^{-1} for $NaFePO_4$ was reported during the first cycle for the battery operated at 60 °C and a C/24 rate, but it quickly decreased to 50.6 mA h g^{-1} in the second cycle and the cyclability was limited to 4–5 cycles.[220,231] A comparative study between olivine $NaFePO_4$ and $LiFePO_4$ with identical physical properties (particle size, particle size distribution, surface coating, and active material loading, etc.) confirms the different thermodynamics and kinetics. The slow sodium ion kinetics in $NaFePO_4$ is considered to be due to a number of factors; i) the Na ions diffusion coefficient is 1-2 magnitude lower than Li, ii) much poorer electronic conductivity and iii) larger volume change in $NaFePO_4$/$FePO_4$ (Fig. 19). [232]

5.2. Triphylite and Maricite $NaFePO_4$

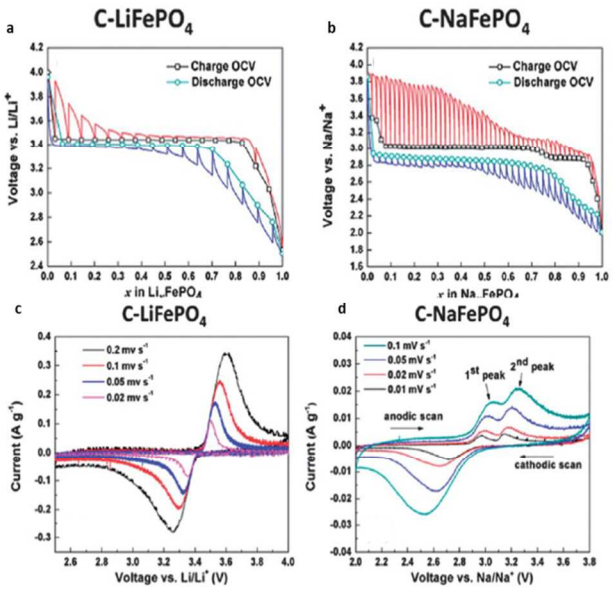

Fig. 19 (a-b) Equilibrium (open-circuit)–voltage (symbols) and transient voltage profiles (solid lines) for C-$LiFePO_4$ and C-Na_xFePO_4. (c-d) Cyclic voltammetry (CV) of C-$LiFePO_4$ in the Li-ion batteries and C-$NaFePO_4$ in the Na-ion batteries. Reproduced with permission from ref. 232. Copyright 2014, the Royal Society of Chemistry.

Different from $LiFePO_4$, $NaFePO_4$ is composed of two different crystal structures, maricite and triphylite (Fig. 20). Maricite $NaFePO_4$ is more thermodynamically stable, but in the maricite $NaFePO_4$ framework, Na^+ and Fe^{2+} occupy the M2 and M1 sites (edge-sharing FeO_6-FeO_6 units), which is the opposite of olivine $LiFePO_4$. As a result, the connectivity of sodium and iron octahedral in this maricite framework blocks the Na ion diffusion channels, limiting Na ion insertion and extraction. In contrast, the metastable triphylite $NaFePO_4$ has corner-sharing FeO_6 units and edge-sharing FeO_6-PO_4. As a result, similar to $LiFePO_4$'s electrochemical behavior, triphylite $NaFePO_4$ allow one-dimensional Na ion diffusion along b direction and can deliver over 120 mAh/g in capacity for sodium-ion batteries. In addition, the electrostatic repulsion between iron and phosphorus also increases Fe-O bond lengths, contributing to a higher redox potential of $FePO_4$/$NaFePO_4$.[233]

Although the maricite $NaFePO_4$ is theoretically electrochemically inactive, a more recent study demonstrates that sodium ions can be extracted/inserted reversibly from maricite $NaFePO_4$ at slow rates. Nevertheless, the delivered capacity is only 1/3 of the theoretical capacity due to the absence of the Na ion diffusion channels. It is evident that further understanding the $NaFePO_4$ structure and the correlating the crystal structure and electrochemical performance is needed to advance this promising material.[218]

5.3. Strategies to electrochemically active $NaFePO_4$

As discussed above, a big challenge in current $NaFePO_4$ research is the synthesis of electrochemically active $NaFePO_4$. Different from $LiFePO_4$, $NaFePO_4$ synthesized by many conventional methods such as classic solid-state routes exhibits poor capacity and irreversibility. This is due to the conventional synthesis methods usually producing the thermodynamically

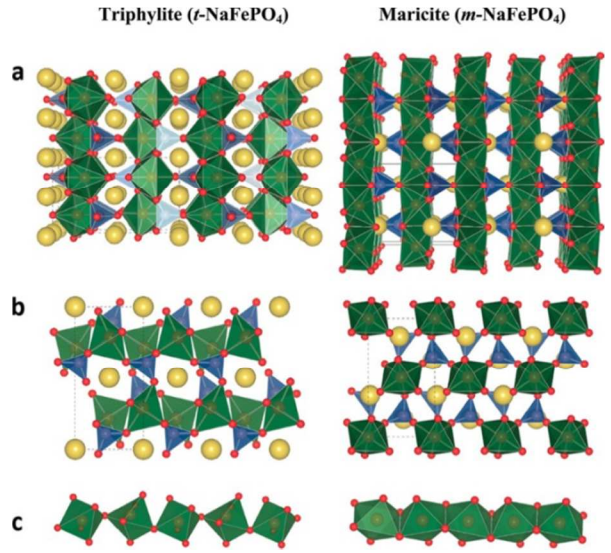

Fig. 20 (a and b) Schematic showing orthorhombic structured triphylite $NaFePO_4$ (left) and maricite $NaFePO_4$ (right). FeO_6 octahedra (green), PO_4 tetrahedra (blue), and Na atoms (yellow). (c) Corner-sharing and edge-sharing coordinations among chains of neighboring FeO_6 octahedra for the two structures. Reproduced with permission from ref. 233. Copyright 2014, American Chemical Society.

stable but electrochemically inactive maricite phase.[234,235] Currently, electrochemically active $NaFePO_4$ with an olivine phase can be mainly obtained via chemical or electrochemical insertion of sodium ions into olivine $FePO_4$.[236-238] In general, this process can be performed through a two-step procedure, involving 1) the delithiation of $LiFePO_4$ in a lithium cell and 2) the use of the delithiated electrode ($FePO_4$) in a new cell, replacing lithium with sodium as the anode. However, for easy handling and safety concerns, it is desirable to use anode materials alternative to sodium metal in practical applications. Similar to a lithium ion battery, Hasa et al reported a new sodium-ion battery with a $NaFePO_4$ cathode and a Sn-C sodium-alloying anode.[239] The $NaFePO_4$ cathode was obtained by Li–Na conversion of a $LiFePO_4$ cathode directly in a full cell with a sodium-ion electrolyte. The results show that this strategy enables efficient conversion of $LiFePO_4$ to $NaFePO_4$ at a voltage of 3 V, resulting in the battery showing a superior maximum capacity of 150 $mAhg^{-1}$, high rate capability and cycle performance.

In addition to the chemical/electrochemical sodiation method, Nazar group recently reported topochemical synthesis of electrochemically active $Na[Mn_{1-x}M_x]PO_4$ (M = Fe, Ca, Mg), where $0<x<0.5$, via a low-temperature solid-state method.[211] In the topochemical reaction, a molten salt reaction converts $NH_4[Mn_{1-x}M_x]PO_4 \cdot H_2O$ (M = Fe, Ca, Mg) to electrochemically active $Na[Mn_{1-x}M_x]PO_4$. Furthermore, the obtained $Na(Fe_{0.5}Mn_{0.5})PO_4$ exhibits a solid solution behavior, which is attributed to the large interface strain due to the large Na ion size. This novel olivine material and synthesis method also opens new opportunities to further develop this olivine cathode for Na-ion batteries.

Another alternative strategy to avoid the direct synthesis of olivine $NaFePO_4$ is by using chemically easily-synthesized $FePO_4$ as the cathode materials for Na-ion batteries.[240-242] Due to its lower processing temperature, amorphous $FePO_4$ is easier to synthesize and exhibits an acceptable electrochemical performance. Furthermore, the isotropic and defect-free nature

of amorphous $FePO_4$ provides a large amount of continuous pathways for Na ions.[243,244] Similar to pristine $LiFePO_4$, $FePO_4$'s conductivity needs to be further improved before its application in sodium-ion batteries. By using carbon nanotubes and graphene, the C/$FePO_4$ composite exhibits an enhanced electrochemical performance.[245,246] Recently, with the functionalization of hodanineacetic acid-pyrene, $FePO_4$ was directly grown on graphene nanosheets. The obtained $FePO_4$/graphene hybrids show superior capacity and rate capability in sodium-ion batteries.[247] Another report involves the synthesis of $FePO_4$ nanospheres via a simple precipitation method. Benefiting from the mesoporous structure and superior carbon conductive network, the C/$FePO_4$ nanospheres exhibit a high initial discharge capacity (151 mAh/g at 20 mA/g rate), a high rate capability (44 mAh g^{-1} at 1000 mA g^{-1}) and a superior cycle stability (94% capacity retention ratio over 160 cycles). [248]

Layered A_2FePO_4F (A=Na, Li) was first reported by Ellis et. al.[249] as a new cathode in either Na-ion and Li-ion batteries. With the layer structure created by interconnected Fe_4F_2-PO_4, this class of materials allow 2D ion diffusion pathways for Na^+ and Li^+, and exhibit a small volume change (3.7%) with negligent stress.[216] The superior structural stability and 2D ion diffusion makes this class of materials promising as the cathode material for both Li ion and Na ion batteries. [250] Furthermore, in contrast to $NaFePO_4$, Na_2FePO_4F can be easily synthesized and electrochemically active. For example, with a common solid state method, the synthesized $NaFePO_4$ is inactive, but Na_2FePO_4F exhibits a discharge capacity of 116 mAh/g at 0.1C with good cycle stability.[251] Therefore, synthesis of Na_2FePO_4F is another possible solution to maricite $NaFePO_4$. In spite of these advantages, the poor electronic conductivity poses big challenges for the practical application of Na_2FePO_4F in sodium ion batteries. To overcome this challenge, similar to $LiFePO_4$, carbon coating, size reduction and nanostructure design strategies are widely applied for the synthesis of high performance Na_2FePO_4F.[252,253]

6. Concluding remarks and future directions

To meet the strict demands of large-scale energy storage systems as found in electric vehicles, lithium ion batteries much achieve high safety, long life time, low cost, high specific capacity, high rate performance and volumetric energy density. Although $LiFePO_4$ is advantageous in terms of safety, life time, cost and specific capacity, the fast charging/discharging property and high volumetric energy density pose critical challenges. Size reduction to the nanoscale is a common strategy to improve rate performance, but meanwhile it also directly lead to a poor volumetric energy density. This is particularly important for $LiFePO_4$, since the theoretical density (3.68 g/cm^3) of $LiFePO_4$ is much lower than many other cathodes (e.g. 5.1 g/cm^3 for $LiCoO_2$, 4.8 g/cm^3 for $LiNiO_2$ and 4.2 g/cm^3 for $LiMn_2O_4$). As a result, the exploration of novel methods, not solely relying on the nano route, is urgently needed to significantly enhance the rate performance while keeping the tap density at acceptable value (such as above 1.5 g/cm^3). The essential breakthrough in finding a high rate performance needs the understanding of the underlying kinetic phase transformation mechanism that is responsible a fast charge/discharge. Recent advances in *in-situ* characterization methods provides direct experimental evidence of solid solution and intermediate phase mechanism during the $LiFePO_4$ phase transformation process under normal operating conditions. This is not the case when using extremely high temperatures (350 ^oC) or small particle sizes (smaller than 40 nm), which drives the design of novel olivine lithium metal phosphate materials with possible solid-solution phase transformation via surface and/or structural modification. This is confirmed by recent findings of the extended solid solution and coherent transformation in $LiMn_{0.4}Fe_{0.6}PO_4$ via *in-situ* synchrotron XRD, which explains the rate capability exceeding $LiFePO_4$'s.[189] In addition, to meet the high volumetric energy density, development of new synthesis routes to produce a micron-scale $LiFePO_4$ secondary structures while maintaining its rate performance are still expected. Current secondary-particle technology allows the tight packing of primary nanoparticles to increase tap densities, but further development is still needed.

Understanding the surface chemistry and interface between carbon and $LiFePO_4$ also plays a critical role in lithium intercalation kinetics and material stability. Some surface phase formation is dependent upon the carbon coating process (size-dependent) and storage circumstance (moisture). In addition, practical manufacturing processes of $LiFePO_4$ may be accompanied with the formation of different impurities such as the iron and phosphorus phases, depending on the preparation conditions. These impurities may block the 1D lithium ion diffusion channels, hindering the effective (de)lithiation capability and reducing the capacity. The existence of these small amounts of impurities also may "poison" $LiFePO_4$ as it can degrade the surface chemistry stability, storage stability and aging process. In addition, the material's homogeneity and production costs are important factors in its large-scale application for EVs. Development of an inexpensive synthesis process by simplifying the processing steps/time, reducing energy consumption and selecting cheap raw materials accelerates the feasibility of $LiFePO_4$ for application. The newly developed molten state method provides an economic and effective route to achieve these goals. [165, 213,254]

Another future research trend is the extension of $LiFePO_4$ to another olivine family, mainly $LiMnPO_4$ due to its high operating voltage (4.1 V vs Li^+/Li) and the accessible electrolyte voltage windows. However, the poorer electron, ion conductivity and Jahn-Teller distortion in $LiMnPO_4$ leads to a limited capacity, making it currently uncompetitive with $LiFePO_4$. In addition, compared to widely studied $LiFePO_4$, understanding of the phase transformation mechanism, structural change upon cycling and thermal stability of $LiMnPO_4$ are still in their infancy. Some inconsistency has been reported for these two olivine lithium phosphates, therefore, they deserve more comprehensive studies. Furthermore, carbon coating seems to be more difficult for $LiMnPO_4$ due to the poor catalytic effect of Mn. One strategy is to apply core/shell structure $LiMnPO_4$/$LiFePO_4$, which takes full advantage of better carbon coating on $LiFePO_4$.[255-258] In particular, some new coating techniques such as atomic layer deposition for thin and uniform $LiFePO_4$ should be considered.[105] Considering these difficulties, an alternative solution is the development of $LiFe_yMn_{1-y}PO_4$ materials, combining the advantages of iron (easy carbon coating, high accessible capacity and safety) and Mn (high voltage). The presence of a solid solution composition also allows a fast charge/discharge rate for this binary olivine lithium phosphate.

Benefiting from the success of lithium ion batteries, recent research in olivine phosphates has been extended to its sodium analogue, $NaFePO_4$, a cathode material for Na-ion batteries. Nevertheless, the presence of two distinct structure (triplylite and maricite) make it difficult to obtain the desired battery

material, as the thermodynamically stable maricite is electrochemical inactive. Current active $NaFePO_4$ are mainly synthesized by an electrochemical sodiation method, which is not suitable for future large-scale production. Therefore, a simple and feasible chemical method to directly synthesize electrochemically active $NaFePO_4$ is highly needed, but is very challenging. With regard to these challenges, at this stage, two solutions have been taken. One is the development of amorphous $FePO_4$ with good electrochemical performance that can be prepared via a direct chemical synthesis route, and the other is use of binary metal olivine phosphate such as $Na(Fe_{0.5}Mn_{0.5})PO_4$ that could be obtained directly by a molten salt reaction.[222] Overall, though $NaFePO_4$ is similar to $LiFePO_4$ in some important respects, it still has a long way to have practical application in the energy storage market.

Acknowledgements

This work was supported by Nature Sciences and Engineering Research Council of Canada (NSERC), Canada Research Chair (CRC) Program, Canada Foundation for Innovation (CFI), Ontario Research Fund (ORF), the Canada Light Source (CLS) at University of Saskatchewan, the Canadian Centre for Electron Microscopy (CCEM) at McMaster University, and University of Western Ontario. We gratefully acknowledge to Mr. Craig Langford for his time and help in the discussion and English polishing for this paper.

Notes and references

[a] Department of Mechanical and Materials Engineering, University of Western Ontario, London, Ontario, N6A 5B9, Canada.
E-mail: xsun@eng.uwo.ca; Tel: +1 5196612111ext. 87759
† Present address: National Synchrotron Light Source II, Brookhaven National Laboratory, Upton, NY, 11973.

1. A. K. Padhi, K. S. Nanjundaswamy and J. B. Goodenough, *J. Electrochem. Soc.*, 1997, **144**, 1188–1194.
2. Y. Wang, P. He, H. Zhou, *Energy Environ. Sci.* 2011, **4**, 805–817.
3. D. Li, H. Zhou, *Materials Today*, 2014, **17**, 451–463.
4. J. B. Goodenough, K. S. Park, *J. Am. Chem. Soc.*, 2013, **135**, 1167 – 1176.
5. L. X. Yuan, Z. H. Wang, W. X. Zhang, X. L. Hu, J. T. Chen, Y. H. Huang, J. B. Goodenough, *Energy Environ. Sci*. 2011, **4**, 269–284.
6. C. Delacourt, P. Poizot, S. Levasseur, and C. Masquelier, *Electrochem. Solid-State Lett*. 2006, **9**, A352–A355.
7. H. Huang, S. C. Yin, L. F. Nazar, *Electrochem. Solid-State Lett.* 2001, **4**, A170–A172.
8. N. Ravet, Y. Chouinard, J. F. Magnan, S. Besner, M. Gauthier and M. Armand, *J. Power Sources*, 2001, **97–98**, 503–507
9. K. Zaghib , M. Dontigny, A. Guerfi, P. Charest, I. Rodrigues, A. Mauger, C.M. Julien, *J. Power Sources* 196, **8**, 3949–3954.
10. L. Laffont , C. Delacourt , P. Gibot, M. Yue Wu, P. Kooyman, C. Masquelier, and J. Marie Tarascon, *Chem. Mater*. 2006, **18**, 5520–5529.
11. D. Morgan, A. Van der Ven, G. Ceder, Electrochem. *Solid-State Lett.* 2004, **7**, A30–A32.
12. Y. Wu, Z. Wen, J. Li, *Adv. Mater*. 2011, **23**, 1126–1129.
13. M. S. Islam, D. J. Driscoll, C. A. J. Fisher, P. R. Slater, *Chem. Mater*. 2005, **17**, 5085–5092.
14. X. J. Wang , H. Y. Chen, X. Yu , L. Wu , K. –W. Nam, J. Bai, H. Li, X. Huang and X.-Q. Yang, *Chem. Commun.* 2011, **47**, 7170–7172.
15. X. Yu, Q. Wang, Y. Zhou, H. Li, X. –Q. Yang, K. –W. Nam, S. N. Ehrlich, S. Khalid and Y. S. Meng, *Chem. Commun*. 2012, **48**, 11537–11539.
16. N. Sharma, V. K. Peterson, M. M. Elcombe, M. Avdeev, A. J. Studer, N. Blagojevic, R. Yusoff, N. Kamarulzaman, *J. Power Sources,* 2010, **195**, 8258–8266.
17. Y. Orikasaa, T. Maeda, Y. Koyama, T. Minato, H. Murayama, K. Fukuda, H. Tanida, H. Arai, E. Matsubara, Y. Uchimoto, and Z. Ogumi. *J. Electrochem. Soc*. 2013, **160**, 3061–3065.
18. C.M. Wang, W. Xu, J. Liu, D.W. Choi, B. Arey, L.V. Saraf, J.G. Zhang, Z.G. Yang, S. Thevuthasan, D.R. Baer and N. Salmon. *J. Mater. Research*. 2011, **25**, 1541–1547.
19. R. Malik, F. Zhou, G. Ceder. *Nat. Mater*. 2011, **10**, 587–590.
20. P. Bai, D. A. Cogswell, and M. Z. Bazant, *Nano Lett*. 2011, **11**, 4890–4896.
21. N. Sharma, X. Guo, G. Du, Z. Guo, J. Wang, Z. Wang, and V. K. Peterson, *J. Am. Chem. Soc.* 2012, **134**, 7867–7873.
22. M. Wagemaker, D. P. Singh, W. J. H. Borghols, U. Lafont, L. Haverkate, V. K. Peterson, and F. M. Mulder, *J. Am. Chem. Soc.,* 2011, **133**, 10222–10228
23. M. Safari, and C. Delacourt, *J. Electrochem. Soc*. 2011, **158**, 1123–1135.
24. Y. Zhang, C. Y. Wang, X. Tang, *J. Power Sources*, 2011, **196**, 1513–1520.
25. C. M. Julien, A. Mauger, K. Zaghib, *J. Mater. Chem*., 2011, **21**, 9955–9968
26. L. Castro, R. Dedryvère, J.-B. Ledeuil, J. Bréger, C. Tessier, and D. Gonbeau, *J. Electrochem. Soc*. 2012, **159**, 357–363.
27. V. Palomares, P. Serras, I. Villaluenga, K. B. Hueso,a J. Carretero-González and T. Rojo, *Energy Environ. Sci.*, 2012, **5**, 5884–5901
28. S. P. Ong, V. L. Chevrier, G. Hautier, A. Jain, C. Moore, S. Kim, X. Ma and G. Ceder, *Energy Environ. Sci*., 2011,**4**, 3680–3688
29. M. Casas-Cabanas, V. V. Roddatis, D. Saurel, P. Kubiak, J. Carretero-González, V. Palomares, P. Serras and T. Rojoa, *J. Mater. Chem.*, 2012, **22**, 17421–17423
30. P. Moreau, D. Guyomard, J. Gaubicher and F. Boucher, *Chem. Mater*., 2010, **22** (14), 4126–4128
31. J. Wang, X. Sun, *Energy Environ. Sci.,* 2012,5, 5163-5185
32. J. D. Wilcox, M. M. Doeff, M. Marcinek, and R. Kostecki, *J. Electrochem. Soc.* 2007, **154**, 389–395.
33. J. D. Wilcox, M.M. Doeff, M. Marcinek, and R. Kostecki, *Solid State Ionics,* 2008, **179**, 1810–1815.
34. Y. Wang, R. Mei, X. Yang, *Ceramics International* 2014, **40**, 8439–8444.
35. Z. -X. Chi, W. Zhang, F.-Q. Cheng, J.-T. Chen, A.-M. Cao and L.-J. Wan, *RSC Adv.*, 2014, **4**, 7795–7798
36. J. Chen, Y.-C. Zou, F. Zhang, Y. –C. Zhang, F.-F. Guo, G.-D. Li, *J. Alloys and Compounds* 2013, **563**, 264–268
37. A. Ponrouch, A. R. Goñi, M. T. Sougrati, M. Ati, J. –M. Tarascon, J. Nava-Avendañoad, M. R. Palacín, *Energy Environ. Sci.,* 2013, **6**, 3363–3371
38. S. Yoon, C. Liao, X. G. Sun, C. A. Bridges, R. R. Unocic, J. Nanda, S. Dai, M. P. Paranthaman, *J. Mater. Chem.* 2012, **22**, 4611–4614.
39. J. Yang, J. Wang, X. Li, D. Wang, J. Liu, G. Liang, M. Gauthier, Y. Li, D. Geng, R. Li, X. Sun. *J. Mater. Chem*., 2012, **22**, 7537–7543.

40. X. L. Yang, G. Peng, L. L. Zhang, G. Liang, S. Duan, Y. H. Huang, A. Lgnatov, M. C. Croft. *J. Electrochem. Soc*. 2012, **159**(12) A2096–A2099.
41. Y. Jin, C. P. Yang, X. H. Rui, T. Cheng, C. H. Chen, *J. Power Sources,* 2011, **196**, 5623–5630.
42. Y. Qu, J. Cao, R. Guo, W. Xu, *Electrochem. Solid State Lett.* 2012, **15(2)**, A15–A18.
43. Z. Ma, G. Shao, X. Qin, Y. Fan, G. Wang, J. Song, T. Liu, *J. Power Sources*, 2014, **269**, 194–202.
44. S. X. Zhao, H. Ding, Y. C. Wang, B. H. Li, C. W. Nan, *J. Alloy Compound* 2013, **566**, 206–211.
45. F. Cheng, S. Wang, A.-H. Lu, W. -C. Li, *J. Power Sources*, 2013, **229**, 249–257.
46. H. D. Asfaw, M. R. Roberts, C. –W. Tai, R. Younesi, M. Valvo, L. Nyholm and K. Edström, *Nanoscale*, 2014, **6**, 8804–8813
47. H. Ni, J. Liu, L. Z. Fan, *Nanoscale*, 2013, **5**, 2164–2168.
48. J. Zhao, J. He, J. Zhou, Y. Guo, T. Wang, S. Wu, X. Ding, R. Huang, H. Xue, *J. Phys. Chem. C*. 2011, **115**, 2888–2894.
49. C. Sun , S. Rajasekhara , J. B. Goodenough, F. Zhou, *J. Am. Chem. Soc.* 2011, **133**, 2132–2135.
50. J. Zhou, H. Liu, Z. P. Li, *Solid State Ionics* 2013, **244**, 23–29.
51. Y. Shi, S. L. Chou, J. Z. Wang, D. Wexler, H. J. Li, H, K. Liu, Y. Wu, *J. Mater. Chem.* 2012, **22**, 16465–16470.
52. X. Zhou, F. Wang, Y. Zhu, Z. Liu, *J. Mater. Chem.* 2011, **21**, 3353–3358.
53. W. T. Geng, D. H. Ping, J. Nara, T. Ohno, *J. Phys. Chem. C* 2012, **116**, 17650–17656.
54. C. Su, X. Bu, L. Xu, J. Liu, C. Zhang, *Electrochimica Acta* 2012, **64**, 190–195.
55. Y. Zhang, W. Wang, P. Li, Y. Fu, X. Ma, *J. Power Sources*, 2012, **210**, 47–53.
56. W. Wei, W. Lv, M. B. Wu, F. Y. Su, Y. B. He, B. Li, F. Kang, Q. H. Yang, *Carbon* 2013, **57**, 530–533.
57. D. Zhao, Y. L. Feng, Y. G. Wang, Y. Y. Xia, *Electrochimica Acta* 2013, **88**, 632–638.
58. L. Hu, F. Wu, C. Lin, A. N. Khlobystov, L. Li, *Nat. Commun*. 2013, **4**, 1687.
59. Y. Liang, D. Wu, X. Feng, K. Müllen, *Adv. Mater*. 2009, **21**, 1679–1683.
60. C. E. Hamilton, J. R. Lomeda, Z. Sun, J. M. Tour and A. R. Barron, *Nano Lett.* 2009, **9**(10), 3460–3462.
61. J. Yang, J. Wang, Y. Tang, D. Wang, X. Li, Y. Hu, R. Li, G. Liang, T. -K. Sham and X. Sun, *Energy Environ. Sci*., 2013, **6**, 1521–1528
62. H. R. Byon, B. M. Gallant, S. W. Lee, Y. Shao-Horn, *Adv. Func. Mater*. 2013, **23**, 1037–1045.
63. Y. Li, Y. Zhao, H. Cheng, Y. Hu, G. Shi, L. Dai, L. Qu, *J. Am. Chem. Soc*. 2012, **134**, 15–18.
64. W. Chen, L. Yan, P. R. Bangal, *Carbon,* 2010, **48**, 1146–1152.
65. Q. B. Zheng, M. M. Gudarzi, S. J. Wang, Y. Geng, Z. Li, J.-K. Kim, *Carbon*, 2011, **49**, 2905–2916.
66. Z. Wang, D. Xu, Y. Huang, Z. Wu, L. Wang, X. Zhang, *Chem. Commun.* 2012, **48**, 976–978.
67. Q. Fan, L. Lei, X. Xu, G. Yin, Y. Sun, *J. Power Sources* 2014, **257**, 65–69.
68. Y. Zhang, W. Wang, P. Li, Y. Fu, X. Ma, *J. Power Sources*, 2012, **210**, 47–53.
69. S. W. Oh, Z. D. Huang, B. Zhang, Y. Yu, Y. B. He, J. -K. Kim. *J. Mater. Chem*. 2012, **22**, 17215–17221.
70. Y. Ding, Y. Jiang, F. Xu, J. Yin, H. Ren, Q. Zhuo, Z. Long, P. Zhang, *Electrochem. Commun.* 2010, **12**, 10–13.
71.T. Lin, J. Chen, H. Bi, D. Wan, F. Huang, X. Xie, M. Jiang, *J. Mater. Chem*. 2013, **1**, 500–504.
72. K. R. Paton, et al. *Nat. Mater*. 2014, **13**, 624–630.
73. S. Praneetha, A. Vadivel Murugan, *RSC Adv.*, 2013, **3**, 25403–25409.
74. B. Wang, D. Wang, Q. Wang, T. Liu, C. Guo, and X. Zhao, *J. Mater. Chem.* A, 2013, **1**, 135–144.
75. J. Li, L. Zhang, L. Zhang, W. Hao, H. Wang, Q. Qu, H. Zheng, *J. Power Sources*, 2014, **249**, 311–319.
76. W. B. Luo, S. L. Chou, Y. C. Zhai, H. K. Liu, *J. Mater. Chem. A*. 2014, **2**, 4927–4931.
77. J. Ha, S. K. Park, S. H. Yu, A. J., B. Jang, S. Bong, I. Kim, Y. E. Sung, Y. Piao, *Nanoscale*, 2013, **5**, 8647–8655.
78. Y. Zhou, J. Wang, Y. Hu, R. O'Hayre, Z. Shao, *Chem. Commun.* 2010, **46**, 7151–7153.
79. M. Chen, C. Du, B. Song, K. Xiong, G. Yin, P. Zuo, X. Cheng, *J. Power Sources*, 2013, **223**, 100–106.
80. J. P. Jegal, K. B. Kim, *J. Power Sources*, 2013, **243**, 859–864.
81. P. Manikandan , P. Periasamy, R. Jagannathan, *J. Mater. Chem. A*, 2013, **1**, 15397–15405.
82. G. Qin, Q. Wu, J. Zhao, Q. Ma, C. Wang, *J. Power Sources*, 2014, **248**, 588–595.
83. L. Dimesso, C. Spanheimer, W. Jaegermann, Y. Zhang, A. L. Yarin, *J. Appl. Phys*. 2012, **111**, 064307.
84. L. Dimesso, C. Förster, W. Jaegermann, J. P. Khanderi, H. Tempel, A. Popp, J. Engstler, J. J. Schneider, A. Sarapulova, D. Mikhailova, L. A. Schmitt, S. Oswald and H. Ehrenberg, *Chem. Soc. Rev*., 2012, **41**, 5068–5080.
85. C. Gong, Z. Xue, X. Wang, X. P. Zhou, X. L. Xie, Y. W. Mail, *J. Power Sources*, 2014, **246**, 260–268.
86. J. Yang, J. Wang, Y. Tang, D. Wang, B. Xiao, X. Li, R. Li, G. Liang, T. K. Sham, X. Sun, *J. Mater. Chem. A*. 2013, **1**, 7306–7311.
87. G. Wang, H. Liu, J. Liu, S. Qiao, G. M. Lu, P. Munroe, H. Ahn, *Adv. Mater*. 2010, **22**, 4944–4948.
88. R. Wu, G. Xia, S. Shen, F. Zhu, F. Jiang, J. Zhang, *RSC Adv*. 2014, **4**, 21325–21331.
89. T. Wumair, J. Dou, L. Zhang, M. Chen, X. Kang, *Ionics*, 2013, **19**, 1855–1860.
90. J. Zhu, J. Fiore, D. Li, N. M. Kinsinger, Q. Wang, E. DiMasi , J. Guo, D. Kisailus, *Cryst. Growth Des.,* 2013, **13**, 4659–4666
91. Z. Ma, G. Shao, Y. Fan, G. Wang, J. Song, and T. Liu, *ACS Appl. Mater. Interfaces*, 2014, **6** (12), 9236–9244.
92. X. Qin, J. Wang, J. Xie, F. Li, L. Wen, X. Wang, Phys. *Chem. Chem. Phys*., 2012, **14**, 2669–2677.
93. K. M. Ø. Jensen, M. Christensen, H. P. Gunnlaugsson , N. Lock, E. D. Bøjesen, T. Proffen, B. B. Iversen, *Chem. Mater.,* 2013, **25** (11), 2282–2290
94. M. Y. Cho, K. B. Kim, J. W. Lee, H. Kim, H. Kim, K. Kang, K. C.Roh, *RSC Adv.,* 2013, **3**, 3421–3427.
95. L. Wang, F. Zhou, Y. S. Meng, G. Ceder, *Phys. Rev. B* 2007, **76**, 165435.
96. K. Saravanan, P. Balaya, M. V. Reddy, B. V. R. Chowdari c, J. J. Vittal, *Energy Environ. Sci.,* 2010, **3**, 457–463.
97. R. Mei, X. Song, Y. Yang, Z. An, J. Zhang, *RSC. Adv*. 2014, **4**, 5746–5752.
98. K. A. Persson, B.Waldwick, P. Lazic, G. Ceder, *Phys. Rev. B.* 2012, **85**, 235438.
99. C. Nan, J. Lu, C. Chen, Q. Peng, Y. Li, *J. Mater. Chem.* 2011, **21**, 9994–9996.

100. W. Kang, C. Zhao, R. Liui, F. Xu, Q. Shen, *CrystEngComm*, 2012, **14**, 2245–2250.
101. Y. Zhao, L. Peng, B. Liu, G. Yu, *Nano Lett.* 2014, **14(5)** 2849–2853.
102. B. Guo, H. Ruan, C. Zheng, H. Fei, M. Wei, *Sci. Rep.* 2013, **3**, 2788.
103. Y. Wang, Y. Wang, E. Hosono, K. Wang, H. Zhou, *Angew. Chem. Int. Ed.* 2008, **47**, 7461–7465.
104. X. Zhang, Z. Bi, W. He, G. Yang, H. Liu, Y. Yue, *Energy Environ. Sci.* 2014, **7**, 2285–2294.
105. J. Liu, M. N. Banis, Q. Sun, A. Lushington, R. Li, T. K. Sham, X. Sun. *Adv. Mater*. 2014, **26**, 6472–6477.
106. J. Du, L. Jiao, Q. Wu, Y. Liu, Z. Qi, L. Guo, Y. Wang, H. Yuan, *Electrochim Acta* 2013, **98**, 288–293.
107. S. Ju, T. Liu, H. Peng, G. Li, K. Chen, *Mater. Lett*. 2013, **93**, 194–198.
108. J. K. Kim, *CrystEngCommun.* 2014, **16**, 2818–2822.
109. F. Yu, S. Lim, Y. Zhen, Y. An, J. Lin, *J. Power Sources* 2014, **271**, 223-230.
110. Y. Jiang, S. Liao, Z. Liu, G. Xiao, Q. Liu, H. Song, *J. Mater. Chem. A*, 2013, **1**, 4546–4551.
111. M. Y. Cho, H. Kim, H. Kim, Y. S. Lim, K. B. Kim, J. W. Lee, K. Kang, K. C. Roh, *J. Mater. Chem. A*, 2014, **2**, 5922–5927.
112. W. K. Kim, W. H. Ryu, D. W. Han, S. J. Lim, J. Y. Eom, H. S. Kwon, *ACS Appl. Mater. Interfaces,* 2014, **6** (7), 4731–4736.
113. M. E. Schuster, D. Teschner, J. Popovic, N. Ohmer, F. Girgsdies, J. Tornow, M. G. Willinger, D. Samuelis, M. –M.Titirici, J. Maier, and R. Schlögl, *Chem. Mater*., 2014, **26** (2), 1040–1047.
114. W. Sigle, R. Amin, K. Weichert, P. A. van Akena, J. Maier, *Electrochem. Solid-State Lett.* 2009, **12**, A151–A154.
115. L. Laffont , C. Delacourt , P. Gibot , M. Y. Wu , P. Kooyman , C. Masquelier , and J. Marie Tarascon, *Chem. Mater*., 2006, **18** (23), 5520–5529.
116. S.Y. Chung, J. T. Bloking, Y. M. Chiang, *Nat. Mater*. 2002, **1**, 123-128.
117. N. Ravet, A. Abouimrane, M. Armand, *Nat. Mater.* 2003, **2**, 702.
118. P. S. Herle, B. Ellis, N. Coombs, L. F. Nazar, *Nat. Mater.* 2004, **3**, 147-152.
119. M. Wagemaker, B. L. Ellis, D. Lutzenkirchen-hecht, F. M. Mulder, L. F. Nazar, *Chem. Mater*. 2008, **20**, 6313–6315
120. N. Meethong, Y. H. Kao, W. C. Carter, Y. M. Chiang, *Chem. Mater*. 2010, **22**, 1088-1097.
121. N. Meethong, Y. H. Kao, S. A. Speakman, Y. M. Chiang, *Adv. Func. Mater*. 2009, **19**, 1060-1070.
122. M. S. Islam, D. J. Driscoll, C. A. J. Fisher, P. R. Slater, *Chem. Mater*. 2005, **17**, 5085-5092.
123. Z. Ma, G. Shao, G. Wang, J. Du, Y. Zhang, *Ionics,* 2013, **19**, 437-443.
124. H. Fang, G. Liang, L. Zhao, T. Wallace, H. Arava, L. L. Zhang, A. Lgnatov, M. C. Croft, *J. Electrochem. Soc.* 2013, **160**, A3148-A3152.
125. A, Moretti, G. Giuli, F. Nobili, A. Trapananti, G. Aquilanti, R. Tossici, R. Marassi, *J. Electrochem. Soc.* 2013, **160**, A940-A949.
126. P. Zhang, Y. Wang, M. Lin, D. Zhang, X. Ren, Q. Yuan, *J. Electrochem. Soc.* 2012, **159**, A402-A409.
127. J. Hong, X. L. Wang, Q. Wang, F. Omenya, N. A. Chernova, M. S. Whittingham, J. Graetz, *J. Phys. Chem. C.* 2012, **116**, 20787-20793.
128. L. L. Zhang, G. Liang, A. Ignatov, M. C. Croft, X. Q. Xiong, I. M. Hung, Y. H. Huang, X. L. Hu, W. X. Zhang, Y. L Peng, *J. Phys. Chem. C*. 2011, **115**, 13520-13527.
129. F. Omenya, N. A. Chernova, S. Upreti, P. Y. Zavalij, K. W. Nam, X. Q. Yang, M. S. Whittingham, *Chem. Mater*. 2011, **23**, 4733-4740.
130. F. Omenya, N. A. Chernova, R. Zhang, J. Fang, Y. Huang, F. Cohen, N. Dobrzynski, S. Senanayake, W. Xu, M. S. Whittingham, *Chem. Mater*. 2013, **25**, 85-89.
131. F. Omenya, N. A. Chernova, Q. Wang, R. Zhang, M. S. Whittingham, *Chem. Mater.* 2013, **25**, 2691-2699.
132. K. L. Harrison, C. A. Bridges, M. P. Paranthaman, C. U. Segre, J. Katsoudas, V. A. Maroni, J. C. Idrobo, J. B. Goodenough, A. Manthiram, *Chem. Mater*. 2013, **25**, 768-781.
133. C. Li, N. Hua, C. Wang, X. Kang, T. Wumair, Y. Han, *J. Alloy Compound*, 2011, **509**, 1897-1900.
134. Q. Liu, Z. Liu, G. Xiao, S. Liao, *Ionics*, 2013, **19**, 445-450.
135. O. Čech, J. E. Thomas, A. Visintin, M. Sedlarikova, J. Vondráke, S. Moreno, *ECS Trans.* 2012, **40**, 93-98.
136. B. Wang, B. Xu, T. Liu, P. Liu, C. Guo, S. Wang, Q. Wang, Z. Xiong, D. Wang, X. S. Zhao, *Nanoscale*, 2012, **6**, 986-995.
137. H. Zhang, Y. Tang, J. Shen, X. Xin, L. Cui, L. Chen, C. Ouyang, S. Shi, L. Chen, *Appl. Phys. A*, 2011, **104**, 529-537.
138. F. Omenya, B. Wen, J. Fang, R. Zhang, Q. Wang, N. A. Chernova, J. Schneider-Haefner, F. Cosandey, M, S, Whittingham, *Adv. Energy Mater.* 2014, DOI: 10.1002/aenm.201401204
139. J. Ni, Y. Zhao, J. Chen, L. Gao, L. Lu, *Electrochem. Commun*. 2014, **44**, 4-7.
140. Z. H. Wang, L. X. Yuan, M. Wu, D. Sun, Y. H. Huang, *Electrochimica Acta,* 2011, **56**, 8477-8483.
141. F. Lu, Y. Zhou, J. Liu, Y. Pan, *Electrochimica Acta*, 2011, **56**, 8833-8838.
142. N. N. Bramnik, K. Nikolowski, C. Baehtz, K.G. Bramnik, and H. Ehrenberg, *Chem. Mater.* 2007, **19**(4) 908–915.
143. M. Okubo, D. Asakura, Y. Mizuno, J.-D. Kim, T. Mizokawa, T. Kudo, and I. Honma, *J. Phys Chem. Lett*. 2010, **1**(14) 2063–2071.
144. A. Yamada, H. Koizumi, N. Sonoyama, R. Kanno, *Electrochem. Solid-State Lett.* 2005, **8** (8), A409–A413.
145. C. Delmas, M. Maccario, L. Croguennec, F. Le Cras, F. Weill, *Nat. Mater.* 2008, **7**, 665–671.
146. D. Burch, M. Z. Bazant, *Nano Lett.* 2009, **9**(11) 3795–3800.
147. T, Sasaki, Y. Ukyo, P. Novak, *Nat. Mater.* 2013, **12**, 569–575.
148. A. S. Andersson, J. O. Thomas*, J. Power Sources*, 2001, **97-98**, 498–502.
149. G. Chen, X. Song, T. J. Richardson*, J. Electrochem. Soc.* 2007, **154**, A627–A632.
150. G. Kobayashi, S. Nishimura, M. S. Park, R. Kanno, M. Yashima, T.Ida, A. Yamada, *Adv. Func. Mater*. 2009, **19**, 395–403.
151. U. S. Kasavajjula, C. Wang, P. E. Arce, *J. Electrochem. Soc*. 2008, **155**, A866–A874.
152. L. J. M. Davis, I. Heinmaa, B. L. Ellis L. F. Nazar, G. R. Goward, *Phys. Chem. Chem. Phys.,* 2011, **13**, 5171–5177.
153. M. Farkhondeh, M. Safari, M. Pritzker, M. Fowler, Taeyoung Han, Jasmine Wang and C. Delacourt, *J. Electrochem. Soc*. 2014, **161**, A201–A212.
154. R. Malik, A. Abdellahi, G. Ceder, *J. Electrochem. Soc*. 2013, **160**, A3179–A3197.
155. K. Weichert, W.Sigle, P. A. van Aken, J. Jamnik, C. Zhu, R. Amin, T. Acartürk, U. Starke, J. Maier, *J. Am. Chem. Soc.,* 2012, **134**(6) 2988–2992.
156. N. Meethong, H.-Y. S. Huang, S. A. Speakman, W. C. Carter, Y.-M. Chiang, *Adv. Func. Mater.* 2007, **17**, 1115–1123.
157. U. Boesenberg, etl al., *Chem. Mater.* 2013, **25**(9) 1664–1672.

158. W. C. Chueh, F. E. Gabaly, J. D. Sugar, N. C. Bartelt, A. H. McDaniel, K. R. Fenton, K. R. Zavadil, T. Tyliszczak, W. Lai, K. F. McCarty, *Nano Lett.* 2013, **13**(3), 866–872.
159. J. Wang, Y. K. Chen-Wiegart, J. Wang, *Nat. Commun*. 2014, **5**, 4570.
160. G. Chen, X. Song, T. Richardson, Electrochem. Solid State Lett. 2006, **9**, A295–A298.
161. D. A. Cogswell, M. Z. Bazant, ACS Nano 2012, **6**, 2215–2225.
162. N. Meethong, H. Y. S. Huang, W. C. Carter, Y. M. Chiang, Electrochem. Solid-State Lett. 2007, **5**, A134–A138.
163. C. Delacourt, P. Poizot, J. –M. Tarascon, C. Masquelier, Nat. Mater. 2005, **4**, 254–260.
164. F. Zhou, T. Maxisch, and G. Ceder, Phys. Rev. Lett. 2006, **97**, 155704.
165. X. J. Wang, H. Y. Chen, X. Yu, L. Wu, K. W. Nam, J. Bai, X. Huang, X. Q. Yang. Chem. Commun. 2011, **47**, 7170–7172.
166. L. Gu, C. Zhu, H. Li, Y. Yu, C. Li, S. Tsukimoto, J. Maier, Y. Ikuhara, J. Am. Chem. SOc. 2011, **133**(13)4661–4663.
167. P. Gibot, M. Casas-Cabanas, L. Laffont, S. Levasseur, P. Carlach, S. Hamelet, J. –M. Tarascon, C. Masquelier, Nat. Mater. 2008, **7**, 741–747.
168. Y. Zhu, J. W. Wang, Y. Liu, X. Liu, A. Kushima, Y. Liu, Y. Xu, S. X. Mao, J. Li, C. Wang, J. Y. Huang, Adv. Mater. 2013, **11**, 5461–5466.
169. B. Ellis, L. K. Perry, D. H. Ryan, L. F. Nazar, J. Am. Chen. Soc., 2006, **128**(35) 11416–11422.
170. L. Gu, C. Zhu, H. Li, Y. Yu, C. Li, S. Tsukimoto, J. Maier, Y. Ikuhara, J. Am. Chem. Soc. 2011, **133** (13), 4661−4663.
171. L. Suo, W. Han, X. Lu, L. Gu, Y. S. Hu, H. Li, D. Chen, L. Chen, S. Tsukimoto, Y. Ikuhara, Phys. Chem. Chem. Phys. 2012, **14** (16), 5363−5367.
172. C. Zhu, L. Gu, L. Suo, J. Popovic, H. Li, Y. Ikuhara, J. Maier, Adv. Funct. Mater. 2014, **24**, 312–318.
173. X. Zhang, M. van Hulzen, D. P. Singh, A. Brownrigg, J. P. Wright, N. H. van Dijk, M. Wagemaker, Nano Lett. 2014, **14**, 2279−2285.
174. Y. Sun, X. Lu, R. Xiao, H. Li, X. Huang, Chem. Mater. 2012, **24**(24) 4693–4703.
175. J. Niu, A. Kushima, X. Qian, L. Qi, K. Xiang, Y. M. Chiang, J. Li, Nano Lett. 2014, **14**(7) 4005–4010.
176. S. F. Amalraj, D. Aurbach, J. Solid State Electrochem. 2011, **15**, 877–890.
177. X. Liu, W. Yang, Z. Liu, Adv. Mater. 2014, **26**, 7710-7729.
178. J. McBreen, J. Solid State Electrochem. 2009, **13**, 1051–1061.
179. Y. Orikasa, T. Maeda, Y. Koyama, H. Murayama, K. Fukuda, H. Tanida, H. Arai, E. Matsubara, Y. Uchimoto, Z. Ogumi, J. Am. Chem. Soc. 2013, **135**(15) 5497–5500.
180. H. Liu, F. C. Strobridge, O. J. Borkiewicz, K. M. Wiaderek, K. W. Chapman, P. J. Chupas, C. P. Grey, Science, 2014, **344**, DOI: 10.1126/science.1252817
181. J. Zhou, J. Wang, L. Zuin, T. Regier, Y. Hu, H. Wang, Y. Liang, J. Maley, R. Sammynaiken, H. Dai, Phys. Chem. Chem. Phys., 2012, **14**, 9578–9581.
182. T. Muraliganth, A. Manthiram, J. Phys. Chem. C. 2010, **114**(36) 15530–15540.
183. D. B. Ravnsbæk, K. Xiang, W. Xing, O. J. Borkiewicz, K. M. Wiaderek, P. Gionet, K. W. Chapman, P. J. Chupas, and Y.-M. Chiang, Nano Lett. 2014, **14**(3) 1484–1491.
184. F. Omenya, J. K. Miller, J. Fang, B. Wen, R. Zhang, Q. Wang, N. A. Chernova, M, S, Whittingham, Chem. Mater. 2014, **26**, 6206–6212.
185. J. Kim, H. Kim, I. Park, Y. U. Park, J. K. Yoo, K. Y. Park, S. Lee, K. Kang, *Energy Environ Sci.* 2013, **6**, 830–834.
186. Q. Liu, H. He, Z. F. Li, Y. Liu, Y. Ren, W. Lu, J. Lu, E. A. Stach, J. Xie, ACS *Appl. Mater. Interfaces*, 2014, **6**(5) 3282–3289.
187. N. Sharma, X. Guo, G. Du, Z. Guo, J. Wang, Z. Wang, V. K. Peterson, *J. Am. Chem. Soc*., 2012, **134** (18), 7867–7873.
188. W. Dreyer, J. Jamnik, C. Guhlke, R. Huth, J. Moškon, M. Gaberšček, *Nat. Mater.* 2010, **9**, 448–453.
189. M. R. Roberts, A. Madsen, C. Nicklin, J. Rawle, M. G. Palmer, J. R. Owen, A. L. Hector, *J. Phys. Chem. C*, 2014, **118** (13), 6548–6557.
190. D. Robert, T. Douillard, A. Boulineau, G. Brunetti, P. Nowakowski, D. Venet, P. B. Guillemaud, C. Cayron, *ACS Nano*, 2013, **7**(12) 10887–10894.
191. X. Liu, D. Wang, G. Liu, V. Srinivasan, Z. Liu, Z. Hussain, W. Yang, *Nat. Commun*, 2013, **4**, 2568.
192. D. A. Shapiro, et. al. *Nat. Photonics*, 2014, **8**, 765–769.
193. B. Kang, G. Ceder, *Nature* 2009, **458**, 190–193.
194. G. Tan, F. Wu, L. Li, R. Chen, S. Chen, *J. Phys. Chem. C* 2013, **117**, 6013−6021.
195. J. L. Allen, T. Richard Jow , J. Wolfenstine, *Chem. Mater*., 2007, **19** (8), 2108–2111.
196. X. Wang, H. Yoshitake, Y. Masaki, H. Wang, *Electrochimica Acta* 2014, **130**, 532–536.
197. J. Wang, J. Yang, Y. Tang, J. Liu, Y. Zhang, G. Liang, M. Gauthier, Y. K. Chen-Wiegart, M. N. Nanis, X. Li, R. Li, J. Wang, T. K. Sham, X. Sun, *Nat. Commun*. 2014, **5**, 3415.
198. M. Koltypin, D. Aurbach, L. Nazar, B. Ellis, *Electrochem. Solid-State Lett.* 2007, **10**, A40–A44.
199. W. Porcher, P. Moreau, B. Lestriez, S. Jouanneau and D. Guyomard, *Electrochem. Solid-State Lett*. 2008, **11**, A4–A8.
200. M. Koltypin, D. Aurbach, L. Nazar, B. Ellis, *J. Power Sources,* 2007, **174**, 1241–1250.
201. K. Amine, J. Liu, I. Belharouak, *Electrochem. Commun*. 2005, **7**, 669–673.
202. M. Safari, C. Delacourt, *J. Electrochem. Soc*. 2011, **158**, A1436–A1447.
203. M. Dubarry, B. Y. Liaw,, M. S. Chen, S. S. Chyan, K. C. Han, W. T. Sie, S. H. Wu, *J. Power Sources*, 2011, **196**, 3420–3425.
204. H. Song, Z. Cao, X. Chen, H. Lu, M. Jia, Z. Zhang, Y. Lai, J. Li, Y. Liu, *J. Solid State Electrochem.* 2013, **17**, 599–605.
205. J. F. Martin, M. Cuisinier, N. Dupré, A. Yamada, R. Kanno, D. Guyomard, *J. Power Sources,* 2011, **196**, 2155–2163.
206. X. Chen, W. Xu, M. H. Engelhard, J. Zheng, Y. Zhang, F. Ding, J. Qian, J. G. Zhang, *J. Mater. Chem. A*. 2014, **2**, 2346–2352.
207. T. Waldmann, S. Gorse, T. Samtleben, G. Schneider, V. Knoblauch and M. Wohlfahrt-Mehrens, *J. Electrochem. Soc.* 2014, **161**, A1742–A1747.
208. M. B. Pinson, Martin Z. Bazant, *J. Electrochem. Soc*. 2013, **160**, A243–A250.
209. M. Cuisinier, J. F. Martin, N. Dupré, A. Yamada, R. Kanno, D. Guyomard, *Electrochem. Commun.* 2010, **12**, 238–241.
210. W. Porcher, P. Moreau, B. Lestriez, S. Jouanneau, F. Le Cras, D. Guyomard, *Ionics*, 2008, **14**, 583–587.
211. J. Wang, J. Yang, Y. Tang, R. Li, G. Liang, T. K. Sham, X. Sun, *J. Mater. Chen. A* 2013, **1**, 1579–1586.
212. K. Zaghib, A. Mauger, F. Gendron, C. M. Julien, *Chem. Mater.* 2008, **20**(2) 462–469.
213. M. Gauthier, C. Michot, N. Ravet, M. Duchesneaua, J. Dufour, G. Liang, J. Wontcheu, L. Gauthier and D. D. MacNeil, *J. Electrochem. Soc.* 2010, **157**, A453–A462.

214. G. Kear, B. D. Barker, F. C. Walsh, *Corrosion Science* 2004, **46**, 109–135.
215. J. Wang, Y. Tang, J. Yang, R. Li, G. Liang, X. Sun, *J. Power Sources,* 2013, **238**, 454–463.
216. S. A. Channagiri, S. C. Nagpure, S. S. Babua, G. J. Noble, R. T. Hart, *J. Power Sources*, 2013, **243**, 750–757.
217. M. D. Slater, D. Kim, E. Lee, C. S. Johnson, *Adv. Func. Mater*. 2013, **23**, 947–958.
218. V. Palomares, P. Serras, I. Villaluenga, K. B. Hueso, J. Carretero-González, T. Rojo, *Energy Environ. Sci*. 2012, **5**, 5884–5901.
219. S. W. Kim, D. H. Seo, X. Ma, G. Ceder, K. Kang, *Adv. Eergy Mater*. 2012, **2**, 710–721.
220. K. Zaghib, J. Trottier, P. Hovington, F. Brochu, A. Guerfi, A. Mauger, C.M. Julien, *J. Power Sources*, 2011, **196**, 9612–9617.
221. S. M. Oh, S. T. Myung, J. Hassound, B. Scrosati, Y. K. Sun, *Electrochem. Commun*. 2012, **22**, 149–152.
222. K. T. Lee, T. N. Ramesh, F. Nan, G. Botton, and L. F. Nazar, *Chem. Mater*. 2011, **23**(16), 3593–3600.
223. J. Gaubicher, F. Boucher, P. Moreau, M. Cuisinier, P. Soudan, E. Elkaim, D. Guyomard. *Electrochem. Commun*. 2014, **38**, 104–106.
224. P. Moreau, D. Guyomard , J. Gaubicher, F. Boucher, *Chem. Mater*. 2010, **22**(14), 4126–4128.
225. M. Casas-Cabanas, V.V. Roddatis, D. Saurel, P. Kubiak, J. Carretero-Gonzales, V. Palomares, P. Serras and T. Rojo, *J. Mater. Chem*. 2012, **22**, 17421–17423.
226. J. Lu, S. C. Chung, S. Nishimura, A. Yamada, *Chem. Mater*. 2013, **25**(22), 4557–4565.
227. M. Galceran, D. Saurel, B. Acebedo, V. V. Roddatis, E. Martin, T. Rojo, M. Casas-Cabanas, *Phys. Chem. Chem. Phys*. 2014, **16**, 8837–8842.
228. M. Galceran, V. Roddatis, F. J. Zuniga, J. M. Perez-Mato, B. Acebedo, R. Arenal, I. Peral, T. Rojo, M. Casas-Cabanas, *Chem. Mater*. 2014, **26**, 3289–3294
229. J. Sugiyama, H. Nozaki, M. Harada, Y. Higuchi, J. H. Brewer, E. J. Ansaldo, G. Kobayashi, R. Kanno, *Phys. Rev. B*, 2014, **90**, 014426.
230. F. Boucher, J. Gaubicher, M. Cuisinier, D. Guyomard, P. Moreau. *J. Am. Chem. Soc*. 2014, **136**(25), 9144–9157.
231. R. Tripathi, S. M. Wood, M. S. Islam, and L. F. Nazar, *Energy Environ. Sci.*, 2013, **6**, 2257–2264.
232. Y. Zhu, Y. Xu, Y. Liu, X. Luo, C. Wang, *Nanoscale* 2013, **5**, 780–787.
233. M. Avdeev, Z. Mohamed, C. D. Ling, J. Lu, M. Tamaru, A. Yamada, P. Barpanda, *Inorg. Chem*. 2013, **52**, 8685–8693.
234. P. P. Prosini, C. Cento, A. Masci, M. Carewska, *Solid State Ionics*, 2014, **263**, 1–8.
235. H. Pan, Y. S. Hu, L. Chen, *Energy Environ. Sci*., 2013, **6**, 2338–2360.
236. S. Y. Hong, Y. Kim, Y. Park, A. Choi, N. S. Choi, K. T. Lee, *Energy Environ. Sci.,* 2013, **6**, 2067–2081
237. V. Palomares, M. Casas-Cabanas, E. Castillo-Martínez, M. H. Han and T. Rojo, *Energy Environ. Sci.* 2013, **6**, 2312–2337.
238. J. Trottier, P. Hovington, F. Brochu, I. Rodrigues, K. Zaghib, A. Mauger and C. M. Julien, *ECS Trans.* 2011, **35**, 123–128.
239. I. Hasa, J. Hassoun, Y. K. Sun, B. Scrosati, *ChemPhyChem,* 2014, **15**, 2152–2155.
240. P. Moreau, D. Guyomard , J. Gaubicher and F. Boucher, *Chem. Mater*. 2010, **22**(14), 4126–4128.
241. Y. Yin, Y. Hu, P. Wu, H. Zhang, C. Cai, *Chem. Commun*. 2012, **48**, 2137−2139.
242. J. Zhao, Z. Jian, J. Ma, F. Wang, Y. S. Hu, W. Chen, L. Chen, H. Liu, S. Dai, *ChemSusChem*. 2012, **5**, 1495–1500.
243. Y. Liu, Y. Xu, X. Han, C. Pellegrinelli, Y. Zhu, H. Zhu, J. Wan, A. C. Chung, O. Vaaland, C. Wang, and L. Hu, *Nano Lett.* 2012, **12**(11), 5664–5668.
244. Y. S. Hong, K. S. Ryu, Y. J. Park, M. G. Kim, J. M. Lee, S. H. Chang, *J. Mater. Chem*. 2002, **12**, 1870–1874.
245. S. Xu, S. Zhang, J. Zhang, T. Tan, Y. Liu, *J. Mater. Chem. A*, 2014, **2**, 7221–7228.
246. J. P. Jegal, J. G. Kim, K. B. Kim, *Electrochem. Commun*, 2013, **30**, 87–90.
247. Q. Fan, L. Lei, G. Yin, Y. Chen, Y. Sun, *Electrochem. Commun*. 2014, **38**, 120–123.
248. Y. Fang, L. Xiao, J. Qian, X. Ai, H. Yang, Y. Cao, *Nano Lett.* 2014, **14**(6), 3539–3543.
249. B. L. Ellis, W. R. M. Makahnouk, Y. Makimura, K. Toghill, L. F. Nazar. *Nat. Mater*. 2007, **6**, 749–753.
250. W. Song, X. Ji, Z. Wu, Y. Zhu, Y. Yao, K. Huangfu, Q. Chen, C. E. Banks, *J. Mater. Chem. A*. 2014, **2**, 2571–2577.
251. N.V. Kosova, V.R. Podugolnikov, E.T. Devyatkina, A.B. Slobodyuk, *Mater. Res. Bull*. 2014, **60**, 849–857.
252. Y. Kawabe, N. Yabuuchi, M. Kajiyama, N. Fukuhara, T. Inamasu, R. Okuyama, I. Nakai, S. Komana, *Electrochem. Commun*. 2011, **13**, 1225–1228.
253. A. Langrock, Y. Xu, Y. Liu, S. Ehraman, A. Manivannan, C. Wang. *J. Power Sources*, 2013, **223**, 62–67.
254. D. .D. MacNeil, L. Devigne, C. Michot, I. Rodrigues, G. Liang, M. Gauthier, *J. Electrochem. Soc*. 2010, **157**(4), A463–A468.
255. S. M. Oh, Y. K. Sun, *J. Power Sources*, 2013, 244, 663-667.
256. K. Zaghib, M. Trudeau, A. Guerfi, J. Trottier, A. Mauger, R. Veillette, C. M. Julien, *J. Power Sources*, 2012, **204**, 177–181.
257. Y. K. Sun, S. T. Myung, B. C. Park, J. Prakash, I. Belharouak, K. Amine, *Nat. Mater*. 2009, **8**, 320–324.
258. Z. Q. Huo, Y. T. Cui, D. Wang, D. Yue, C. Li, *J. Power Sources*, 2014, **245**, 331–336.

This review highlights the remaining challenges of $LiFePO_4$ in lithium-ion batteries and future olivine cathodes in Na-ion batteries.